University of New Mexico
UNM Digital Repository

Electrical and Computer Engineering ETDs Engineering ETDs

5-14-1968

A Technique For Determining Transistor Spall Thresholds.

Herbert L. Floyd Jr.

Follow this and additional works at: https://digitalrepository.unm.edu/ece_etds

Part of the Electrical and Computer Engineering Commons

THE UNIVERSITY OF NEW MEXICO LIBRARY

MANUSCRIPT THESES

Unpublished theses submitted for the Master's and Doctor's degrees and deposited in the University of New Mexico Library are open for inspection, but are to be used only with due regard to the rights of the authors. Bibliographical references may be noted, but passages may be copied only with the permission of the authors, and proper credit must be given in subsequent written or published work. Extensive copying or publication of the thesis in whole or in part requires also the consent of the Dean of the Graduate School of the University of New Mexico.

This thesis by Herbert L. Floyd, Jr. has been used by the following persons, whose signatures attest their acceptance of the above restrictions.

A Library which borrows this thesis for use by its patrons is expected to secure the signature of each user.

NAME AND ADDRESS	DATE

This dissertation, directed and approved by the candidate's committee, has been accepted by the Graduate Committee of The University of New Mexico in partial fulfillment of the requirements for the degree of Master of Science

A Technique for Determining

Transistor Spall Thresholds

Title

Herbert L. Floyd, Jr.

Candidate

Department of Electrical Engineering

Department

Art Stege

Dean

5-24-68

Date

Committee

Harold D. Southward

Chairman

Harold T. Cates

Arnold H. Koschmann

W. J. Byatt

A TECHNIQUE FOR DETERMINING TRANSISTOR SPALL THRESHOLDS

BY
HERBERT L. FLOYD, JR.
B. E. E., The Ohio State University, 1958

THESIS

Submitted in Partial Fulfillment of the
Requirements for the Degree of
Master of Science in Electrical Engineering
in the Graduate School of
The University of New Mexico
Albuquerque, New Mexico

June, 1968

LD
3781
N563F645
cop. 2

ACKNOWLEDGMENTS

The author is indebted to Lynn M. Barker for his assistance in adapting SWAP-7 to this unusual application and to Robert A. Graham, whose suggestions formed the basis for this study. The counsel and guidance of Prof. Harold D. Southward, University of New Mexico, is also gratefully acknowledged.

481211

A TECHNIQUE FOR DETERMINING TRANSISTOR SPALL THRESHOLDS

BY
Herbert L. Floyd, Jr.

ABSTRACT OF THESIS

Submitted in Partial Fulfillment of the
Requirements for the Degree of
Master of Science in Electrical Engineering
in the Graduate School of
The University of New Mexico
Albuquerque, New Mexico

June, 1968

ABSTRACT

The purpose of the work described in this report was to develop a technique for determining the mechanical robustness of small electronic components when subjected to short-duration stress waves. Techniques employed by other experimenters, which include flyer-plate impaction and pulsed-electron deposition, are difficult to control and to analyze. The procedure described herein overcomes these difficulties by restricting the variables that control accuracy to those which can be precisely measured.

The wave equation was derived and solved for deformable bodies subjected to unidimensional strain. In addition to providing insight into the dependence of high-tensile stresses on stress-wave characteristics and component geometry, these calculations suggested the laboratory technique that was used. Stress waves were generated by depositing a burst of high-energy electrons into an aluminum absorber. The stress wave was acoustically coupled into transistors, which were chosen as the vehicle for this experiment, by clamping the bottoms of their headers to the rear surface of the absorber. Catastrophic mechanical failures were induced in nine out of ten classes of transistors.

Analysis of the experimental results was performed by using a stress-wave-analyzing computer program to simulate the response of the absorber-transistor assembly to the stress input. Using the stress waveform measured by a quartz gauge clamped to the absorber, the computer was programmed to calculate the stresses that prevailed at the locations of observed failure. By varying the amplitude of the input stress, it was possible to determine the threshold of stress that caused failure in nine classes of transistors. These thresholds for all observed failures are tabulated.

Suggestions for refinement of the technique and for its extension to other types of electronic components are made. Examples of the use of the results to increase the robustness of transistors are also presented. Appendix A explains one of the disadvantages of using explosively driven flyer plates to generate stress waves in transistors. Details of the SWAP-7 computer code that are relevant to its use with the reported technique, including formulas necessary for calculating the input data, are presented in Appendix B.

CONTENTS

	Page
Introduction	1
Background	1
Theory	3
Wave Equation	4
Tensile Dependence on Geometry	13
Stress-Wave Generation	16
Experimental Technique	21
Description of Method	21
Experimental Results	26
Analysis	35
Conclusions	46
Appendix A. Flyer-Plate Loading Disadvantages	49
Appendix B. Application of SWAP-7 Computer Code	53
Bibliography	59

LIST OF FIGURES

Figure		Page
1	Cross Section of Thin Disc Showing Area of Unidimensional Strain	5
2	Stress Waves of Different Slopes but Same Peak Stress Incident on Free Surface	14
3	Stress Waves of Figure 2 After Reflection . . .	15
4	Stress Waves of Figure 2 During Reflection . . .	15
5	Profile of Specific Energy Deposited in Aluminum by High-Energy Electrons	18
6	Stress Profile Resulting From Fast Deposition of Energy Shown in Figure 5	19
7	Stress Propagation After Electron Deposition . .	20
8	Stress Wave Produced by Febetron 705 in Aluminum	23
9	Cross Section of Transistor Mounting Assembly .	25
10	Typical Die-Attach Failure	28
11	Typical Silicon-Die Spall	29
12	Typical Die Fracture	30
13	Wire-Die Bond Rupture	32
14	Typical Wire-Post Bond Rupture.	33
15	Example of Compound Failure	34
16	Initial Conditions of SWAP-7 Computer Run . . .	37
17	Stress Amplification by Impedance Mismatch . .	38
18	Absorber-Header Interface Separation	39

LIST OF FIGURES (cont.)

Figure		Page
19	Reflections From Free Surface Begin	40
20	Tensile Reinforcement Near Free Surface . . .	41
21	Die-Attach Spall	42
22	Stress Ringing in Separated Die	43
23	Cross Section of Idealized Transistor	49
24	x-t Plot for Flyer-Plate Impact	50
25	Example of SWAP-7 Input Parameters.	55

LIST OF TABLES

Table		
1	Summary of Results	45
2	Properties Influencing Stress Response	50

ABBREVIATIONS AND SYMBOLS

Symbol	Definition
σ	longitudinal stress under uniaxial strain conditions
x	distance along the axis of uniaxial strain
A	arbitrary area normal to axis of uniaxial strain
ρ	material density under standard atmospheric conditions
u	displacement of material along the axis of uniaxial strain
F	Hugoniot elastic modulus of elasticity
c_o	velocity of sound in a given material
t	time
$G(x, t)$	arbitrary function describing initial displacement
$f, g(x, t)$	arbitrary function describing stress waveform
C	constant of integration or capacitance
ϵ	uniaxial strain
v, U_p	particle velocity
i	current
L	inductance
V	voltage
Z, I	electrical or acoustical impedance
U_s	shock velocity
γ	Grüneisen parameter

ABBREVIATIONS AND SYMBOLS (cont.)

Symbol	Definition
$\bar{a}$	average acceleration
τ	shear stress for uniaxial strain conditions
K	bulk modulus of elasticity
μ	Poisson's ratio

Abbreviation	
CDC 3600	Control Data Corp. Model 3600 computer
SWAP-7	one-dimensional stress-wave-analyzing computer program
NA	analysis not applicable
TOODY	two-dimensional stress-wave-analyzing computer program

A TECHNIQUE FOR DETERMINING TRANSISTOR SPALL THRESHOLDS

Introduction

Most materials tend to fail in tension; however, since it is difficult to place small masses in tension by indirect excitation, semiconductor devices such as transistors and integrated circuits are somewhat impervious to shock and acceleration, in spite of their frangible silicon crystals and tiny soft wires. Short, sonic velocity stress waves, however, can create destructive tensile stresses that have only recently been explored by semiconductor users and manufacturers. This report describes an analytical and experimental technique for determining the response of a large class of devices to such stress waves.

Background

Spallation is defined as the separation of a material or interface resulting from the tension introduced by the interaction of two rarefaction waves.[1] Stress-wave interactions with material boundaries and with

[1] Butcher, B. M.; Barker, L. M.; Munson, D. E.; and Lundergan, C. D., "Influence of Stress History on Time-Dependent Spall in Metals," AIAA Journal, June 1964.

themselves can, under proper conditions, produce a tensile wave. Semiconductor devices, which consist of small active assemblies that represent essentially free-surface extensions of relatively large headers or substrates, restrict these conditions to short-duration stress waves that decay rapidly from a state of compression to one of either zero stress or a tensile condition. This restriction limits the experimental techniques that can be used to study spall phenomena in semiconductor devices.

Computer codes have been written to predict the stress response of structures, subject to certain geometrical limitations, but their usefulness presumes a knowledge of the equations of state and spall thresholds of the materials involved. Since the constituent parameters of these relations for materials used in semiconductors are sensitive to fabrication techniques, geometry, and strain rates, they must usually be determined empirically. This can be done by modeling a device for a stress-wave-analyzing computer program, subjecting the device to a known stress wave, then adjusting the parameters of the program until the results predicted by the code correspond to those observed in the laboratory. Should the code then accurately predict the response to other stress waves, confidence is established in the chosen model and experimental technique.

Development of a satisfactory laboratory technique has been the principal obstacle to this approach. The most commonly used stress-wave-generating techniques, flyer-plate impact and electron-beam deposition, are difficult to analyze and involve associated phenomena that can obscure the desired effects. The limits of reducing the mass and increasing the velocities of flyer plates have been approached without producing a desirable stress wave. Device response measurements are indirect and difficult, and momentum transfer exercises the devices to a degree greater than desired.[2] Direct deposition of high-energy electrons onto the exposed surfaces of transistors is complicated by the effects of the electronic charge buildup and the uncertainty of time dependence of beam spectrum and fluence. The former causes unwanted device degradation and the latter makes it difficult to calculate the generated stress waves. The technique reported on here is an attempt to combine the advantages of these two approaches while eliminating many of the disadvantages.

Theory

In rigid-body dynamics, it is assumed that a force applied to any point of a body will set every other point in motion instantaneously, and the body will respond as an entity to Newton's laws of motion. Elasticity theory considers only the static deformations manifested by bodies in

---

[2] See Appendix A.

equilibrium under the stresses of applied forces. Neither of these treatments is sufficiently accurate to describe the response of deformable bodies to short-duration or rapidly varying stresses. The twofold purpose of this section is to develop a qualitative method for predicting the response and to demonstrate how the application of the method to transistors led to the experimental and analytical technique described in this report.

Wave Equation

Consider a deformable circular disc whose axis lies along the x-axis of a cylindrical coordinate system having radial dimensions sufficiently larger than its axis that unidimensional strain conditions prevail for plane stress waves along the x-axis.[3] The time required for strain waves originating at the radial peripheries to propagate to the x-axis is much greater than the intended time of observation of the stress conditions along the x-axis, so the body is unable to strain in the radial direction. Consider further: (1) a tube of area A concentric with the x-axis in which the initial displacement distribution is G(x) and (2) an element PR of this tube of length ∂x (see Figure 1). If the stress normal to PQ is $\sigma(x)$, then the stress on RS will be

$$\sigma(x) + \left(\frac{\partial\sigma(x)}{\partial x}\right) \partial x.$$

[3] This condition holds for most cases described in this report.

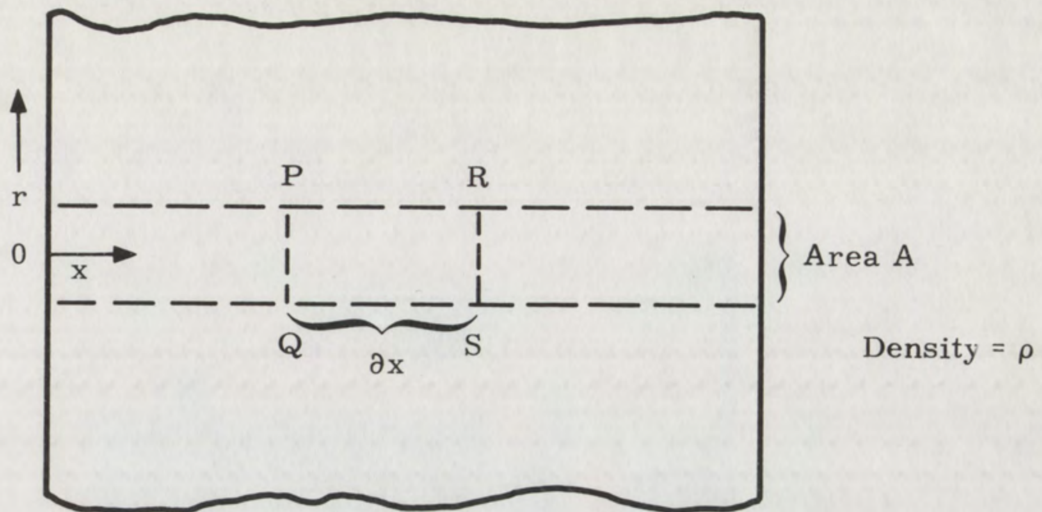

FIGURE 1.
Cross Section of Thin Disc Showing Area of Unidimensional Strain.

Newton's second law of motion describes the displacement, u, of the material in this element as

$$\rho A \partial x \frac{\partial^2 u}{\partial t^2} = A \frac{\partial \sigma(x)}{\partial x} \partial x. \tag{1}$$

In the elastic region, $\sigma(x) = F \frac{\partial u}{\partial x}$ where F is the Hugoniot modulus of elasticity and $\frac{\partial u}{\partial x}$ is the strain. Substituting for $\sigma(x)$ in Equation 1 and simplifying, we obtain

$$\frac{\partial^2 u}{\partial t^2} = \frac{F}{\rho} \frac{\partial^2 u}{\partial x^2}, \tag{2}$$

which is the wave equation for material displacement along the x-axis. D'Alembert's solution to this equation is

$$u(x, t) = f(x + c_o t) + g(x - c_o t), \tag{3}$$

which corresponds to two waves traveling in opposite directions, with constant velocity,

$$c_o = \sqrt{\frac{F}{\rho}}$$

and shapes determined by the initial conditions. If we assume that the initial displacement distribution, $G(x)$, was created without imparting momentum to the disc,[4] the following initial conditions will prevail:

$$u(x, o) = G(x) \tag{4}$$

and

$$mv = \rho A \partial x \frac{\partial u}{\partial t} = 0. \tag{5}$$

Differentiating Equation 3 with respect to t and substituting into Equation 5, we get

$$\rho A \partial x \left[c_o f' (x + c_o t) - c_o g' (x - c_o t) \right] = 0,$$

which holds for all t.

Hence,

$$f' (x + c_o t) - g' (x - c_o t) = 0.$$

For $t = 0$,

$$f' (x) = g' (x).$$

It follows that

$$f(x) = g(x) + C.$$

Because this holds for all x, say $x' = x + c_o t$,

---

[4]This condition holds for most cases described in this report.

then,

$$f(x + c_o t) = g(x + c_o t) + C. \tag{6}$$

Substituting Equation 6 into Equation 3 results in

$$u(x, t) = g(x + c_o t) + g(x - c_o t) + C. \tag{7}$$

Applying the initial condition in Equation 4 to Equation 7, we have

$$u(x, o) = g(x) + g(x) + C = G(x)$$

$$g(x) = \frac{1}{2} G(x) - \frac{1}{2} C \text{ for all x, say } x' = x - c_o t.$$

Therefore,

$$g(x - c_o t) = \frac{1}{2} G(x - c_o t) - \frac{1}{2} C. \tag{8}$$

Similarly,

$$f(x) = \frac{1}{2} G(x) + \frac{1}{2} C \text{ for all x, say } x' = x + c_o t,$$

so that

$$f(x + c_o t) = \frac{1}{2} G(x + c_o t) + \frac{1}{2} C. \tag{9}$$

Substituting Equations 8 and 9 into Equation 3, we get

$$u(x, t) = \frac{1}{2} G(x + c_o t) + \frac{1}{2} C + \frac{1}{2} G(x - c_o t) - \frac{1}{2} C$$

$$u(x, t) = \frac{1}{2} G(x + c_o t) + \frac{1}{2} G(x - c_o t).$$

We see that the solution of the wave equation for the assumed initial conditions consists of two plane waves of the same shape as the initial displacement distribution, but having half the amplitude, traveling in opposite directions at velocity $c_o = \sqrt{\frac{F}{\rho}}$. Because this velocity is constant, both wave shapes will be preserved until perturbing strains

are introduced by relief waves originating at the radial peripheries, at which time unidimensional strain conditions no longer hold.

To extend this solution to that of the wave equation describing stress-wave propagation, consider that the stress in the x-direction is related to the strain and the Hugoniot modulus of elasticity by

$$\sigma(x, t) = F \frac{\partial u(x, t)}{\partial x} = \frac{1}{2} FG' (x + c_o t) + \frac{1}{2} FG' (x - c_o t)$$

where G' denotes differentiation with respect to x. For t = 0, this relation reduces to

$$\sigma(x, 0) = FG' (x).$$

Therefore, we find that the solution to the stress-wave equation consists also of two plane stress waves of the same shape and initial position as the initial stress distribution, but having half the amplitude, traveling at the same constant velocity but in opposite directions.

In order to determine the relationship between particle velocity and stress, consider the wave moving in the direction of decreasing x:

$$u(x, t) = f(x + c_o t). \tag{10}$$

The strain in the x-direction is given by

$$\epsilon(x, t) \equiv \frac{\partial u}{\partial x} = f' (x + c_o t) \tag{11}$$

where f' denotes differentiation by the argument $(x + c_o t)$. The particle velocity is

$$v(x, t) \equiv \frac{\partial u}{\partial t} = c_o f' (x + c_o t). \tag{12}$$

Combining Equations 11 and 12, we get

$$\frac{\partial u}{\partial t} = c_o \frac{\partial u}{\partial x} .$$

But stress is the product of the elastic modulus and the strain, or

$$\sigma(x) = F \frac{\partial u}{\partial x} . \qquad (13)$$

Thus,

$$\sigma(x) = \frac{F}{c_o} \frac{\partial u}{\partial t} ,$$

which indicates that stress is a linear function of particle velocity.

The nature of the reflection of a plane wave from a free surface can now be determined by considering again the wave described in Equation 10 and letting the right free surface of Figure 1 correspond to $x = 0$. If the wave incident on this surface is

$$u_i = f_1 (x + c_o t),$$

then the reflected wave will be

$$u_r = f_2 (x - c_o t).$$

The stresses associated with these two waves, according to Equation 13, will be

$$\sigma_i = F \frac{\partial u_i}{\partial x}$$

and

$$\sigma_r = F \frac{\partial u_r}{\partial x} ,$$

and the total stress will be

$$\sigma(x, t) = \sigma_i + \sigma_r = F\left(\frac{\partial u_i}{\partial x} + \frac{\partial u_r}{\partial x}\right)$$

$$\sigma(x, t) = F\left[f_1'(x + c_o t) + f_2'(x - c_o t)\right]. \tag{14}$$

Because a free surface cannot support a stress, the boundary condition $\sigma(o, t) = 0$ prevails, reducing Equation 14 to

$$\sigma(o, t) = F\left[f_1'(c_o t) + f_2'(-c_o t)\right] = 0.$$

Thus,

$$f'(c_o t) + f_2'(-c_o t) = 0 \tag{15}$$

for all t, say

$$t' = \frac{x}{c_o} - t. \tag{16}$$

Substituting Equation 16 into Equation 15, we get

$$f_2'(x - c_o t) = -f_1'(-x + c_o t). \tag{17}$$

Substituting Equation 17 into Equation 14, we get

$$\sigma(x, t) = F\left[f_1'(x + c_o t) - f_1'(-x + c_o t)\right]. \tag{18}$$

Thus,

$$\sigma_i = F f_1'(x + c_o t)$$

and

$$\sigma_r = -F f_1'(-x + c_o t), \tag{19}$$

which indicates that a free surface will reflect a compressive stress wave as a tensile wave of the same amplitude, shape, and velocity, and

a tensile wave will be reflected as a compressive wave with the same properties. The net stress will be the algebraic sum of the incident and reflected waves.

For the calculation of the stress reflection at an interface between two different materials, it is convenient to take advantage of the analogy between our mechanical system and that of an interface between two lossless electrical transmission lines. Recall that the wave equations for the latter system are:

$$\frac{\partial^2 i}{\partial t^2} = \frac{1}{LC} \frac{\partial^2 i}{\partial x^2}$$

and

$$\frac{\partial^2 V}{\partial x^2} = LC \frac{\partial^2 V}{\partial t^2} .$$

These equations are equivalent to

$$\frac{\partial^2 v}{\partial t^2} = \frac{F}{\rho} \frac{\partial^2 v}{\partial x^2}$$

and

$$\frac{\partial^2 \sigma}{\partial x^2} = \frac{\rho}{F} \frac{\partial^2 \sigma}{\partial t^2}$$

where the following variables are analogous:

particle velocity and current

stress and voltage

density and inductance

Young's modulus and reciprocal capacitance.

By analogy the following parameters can be determined:

(1) From electrical characteristic impedance $Z = \sqrt{\frac{L}{C}}$,

we find acoustical impedance $Z = \sqrt{\rho F}$.

(2) Propagation velocity $u = \sqrt{\frac{1}{LC}}$

implies that stress wave velocity $u_s = \sqrt{\frac{F}{\rho}}$.

(3) The ratio of voltage transmitted to line 2 to the voltage incident on the interface from line 1, defined as the transmission coefficient, is found by

$$\frac{V_T}{V_i} = \frac{2Z_2}{Z_2 + Z_1}$$

where Z_1 and Z_2 are the characteristic impedances of lines 1 and 2, respectively. For the mechanical system, the transmission coefficient is similar:

$$\frac{\sigma_T}{\sigma_i} = \frac{2Z_2}{Z_2 + Z_1}$$

where Z_1 and Z_2 are the acoustical impedances of materials 1 and 2, respectively.

(4) Similarly, the stress reflection coefficient is

$$\frac{\sigma_R}{\sigma_i} = \frac{Z_2 - Z_1}{Z_2 + Z_1} .$$

Applying these last two relations to the reflection of a stress wave at a free surface ($Z_2 = 0$) of a material having acoustical impedance Z_1, we get

$$\frac{\sigma_T}{\sigma_i} = \frac{2Z_2}{Z_2 + Z_1} = 0$$

and

$$\frac{\sigma_R}{\sigma_i} = \frac{Z_2 - Z_1}{Z_2 + Z_1} = -1,$$

which are the same results derived in Equation 19.

Tensile Dependence on Geometry

The generation of a tensile stress wave in a transistor is complicated by the fact that the region of interest, the silicon die, is practically a free surface of the header-die system. Because the stress at a free surface is always zero, it follows that the stress in the die will rise from zero at its surface to a level dependent on the shape of the particular stress wave incident on this surface. It is useful to observe some general effects of this dependency to enable the experimenter to tailor his stress-wave shapes to achieve a particular response.

Consider two right-moving plane waves of the same peak amplitude, but different slopes, propagating through a material in which we seek to maximize the tensile stress near the right free surface. Figure 2 describes the initial conditions and indicates, by a dashed line, the plane where maximum tensile stress is desired.

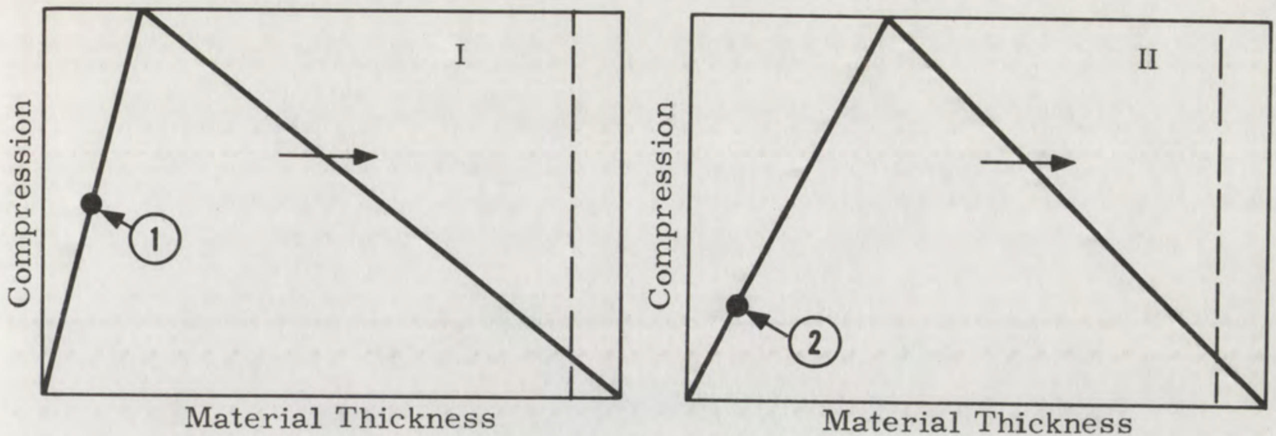

FIGURE 2.
Stress Waves of Different Slopes but Same Peak Stress
Incident on Free Surface.

During reflection by the right free surface, the leading edges of the stress wave will propagate back to the left as tensile waves of the same amplitude, temporarily perturbing the shape of the right-moving compression wave and generally reducing its amplitude. At the conclusion of reflection, however, the original waveform will have been restored, but the material will be in a general state of tension, as shown in the sketches in Figure 3.

If one ignores the stresses during reflection, it might be concluded that the magnitudes of the maximum tensile stresses that appear at points A and B are the same as those of the compression wave at the equivalent distance from the trailing stress nodes (see points 1 and 2 in the first sketches). At a particular time just before the conclusion of reflection, however, the stress waves shown in Figure 4 will result from an optimum addition of the incident and reflected waves.

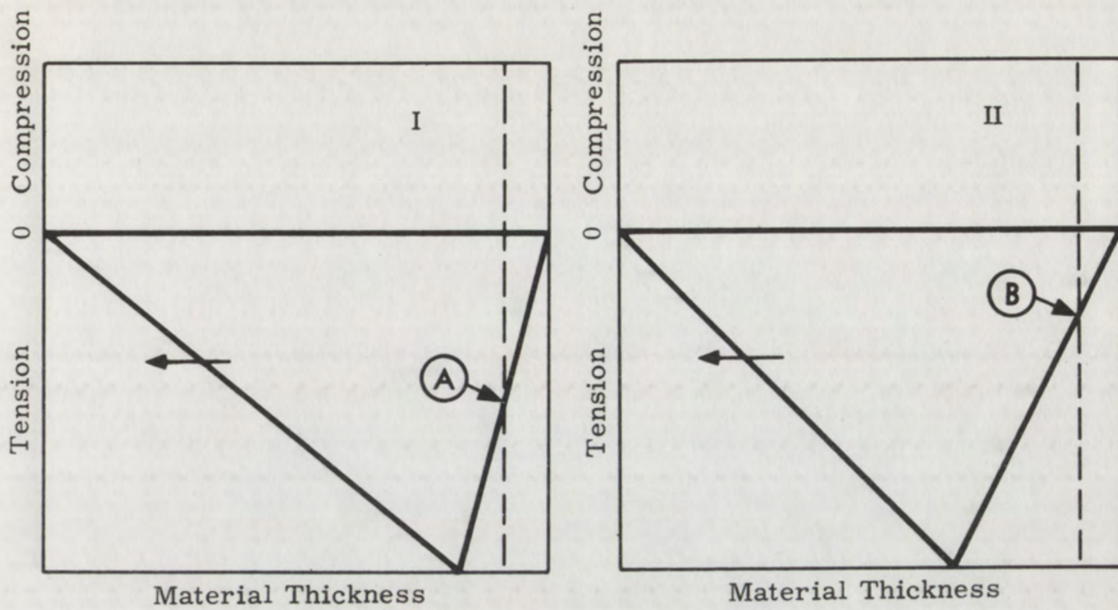

FIGURE 3.
Stress Waves of Figure 2 After Reflection.

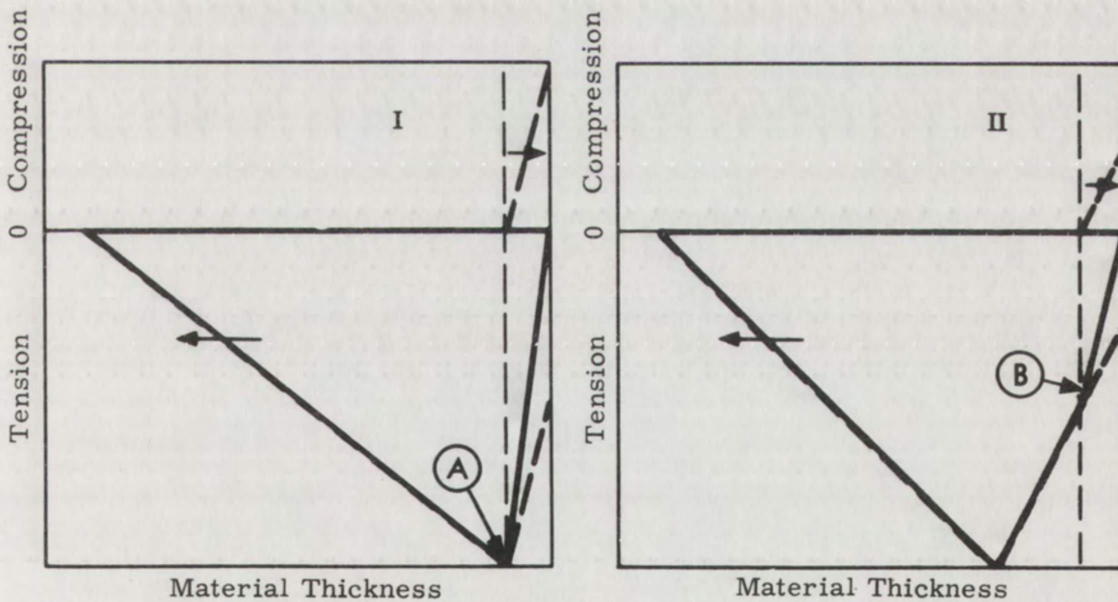

FIGURE 4.
Stress Waves of Figure 2 During Reflection.

Note that the maximum tensile stresses that appear at A and B are twice those that appear at any time except during reflection.

Although it is not rigorously obvious from this cursory observation, a reasonable prediction of the near-surface behavior of stress waves can be made by using the following approximations:

(1) For distances from the free surface less than the distance from the peak of the compression wave to its trailing stress node, the magnitude of the peak tensile stress will be twice that of the compression wave at the same distance from the node.

(2) For distances from the free surface greater than the limit in 1, above, the magnitude of the peak tensile will be equal to that of the peak compression.

(3) For the same distances from the free surface as in 1, above, the magnitude of the peak tensile generated increases with increasing slope of the compression wave from its peak to its node.

Stress-Wave Generation

The study of spall in a deformable body becomes complicated if spurious external stresses are applied to the body during the time that events are building up to a spall condition. Because of the inertia of the

wires suspended between the silicon die and the lead posts of a transistor, the die will be subjected to such external stresses if a velocity is suddenly applied to the device. In the interest of experimental control, then, it behooves the experimenter to introduce his stress waves to his test specimen in such a way that no net momentum is transferred.

The generation of stress waves in a material without attendant momentum transfer precludes the use of impact loading with flyer plates, and the restriction to short pulses having large slopes from maximum to zero stress conditions further reduces the choice of techniques. The method used for the work described in this report takes advantage of the fact that if a material is heated in depth instantaneously it will be unable to expand immediately to a volume commensurate with its temperature, so a compressive stress profile will be established. This profile is described by the Mie Grüneisen equation of state,

$$\sigma = 41.86\, \rho \gamma E,$$

where σ is stress in bars, 41.86 is a dimensional constant, ρ is the material density in gm/cm^3, γ is the Grüneisen parameter (of the order of 2 for most metals), and E is the specific energy in cal/gm at the given point in the material. The vehicle used to create this near-instantaneous increase in internal energy was a burst of high-energy electrons which release their kinetic energy through a collision process that results in a

negligible transfer of momentum. Because of the importance of stress-waveform influence on the results that were observed experimentally, a brief description of the events that led to its formation is presented here.

The thermal energy generated in an absorber by a pulse of high-energy electrons is typically distributed as shown in Figure 5, below.

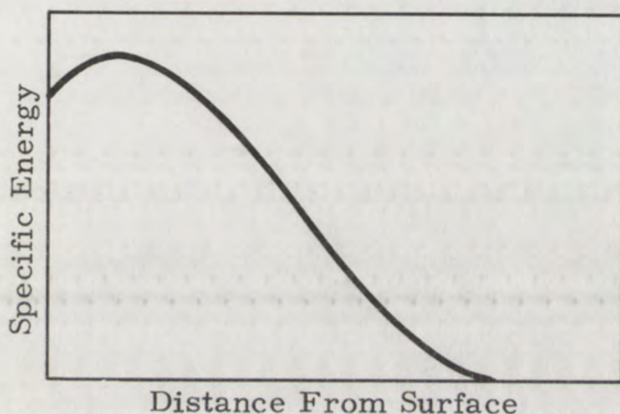

FIGURE 5.
Profile of Specific Energy Deposited in Aluminum by High-Energy Electrons.

The shape of this distribution is a function of the stopping power of the material for electrons having the energies of those in the absorbed pulse. The linearity of the Mie Grüneisen relation suggests that the resulting compressive stress profile will have the same shape as this initial energy distribution. If one considers a finite deposition time, however, an additional restriction must be considered in determining the stress profile at the conclusion of deposition. The front of the absorber, being a free surface, cannot support a stress for a finite time; therefore, during deposition, the stress at this point will be relieved to zero and the stress profile will look more like that shown in Figure 6.

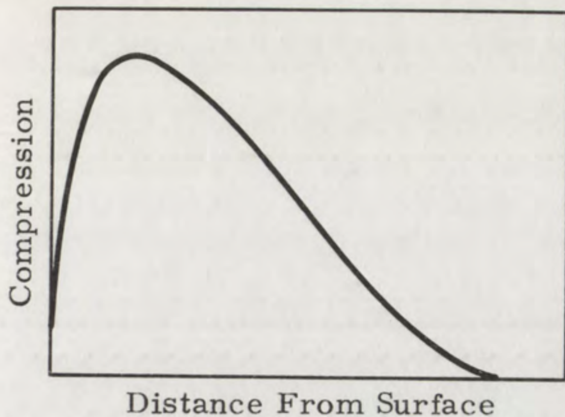

FIGURE 6.
Stress Profile Resulting From
Fast Deposition of Energy
Shown in Figure 5.

Recall that such an initial stress, having been effected with negligible transfer of momentum, will give rise to two half-amplitude stress waves moving at sonic velocity in opposite directions away from the initial stress position and that the net stress at any point and time will be the algebraic sum of these waves. For simple systems, an estimate of the stress propagation can be obtained graphically by approximating these traveling waves with straight-line shapes, plotting them at strategic time intervals while accounting for free-surface reflections, and adding the stresses at times of interest. A typical series of approximations for the conditions under discussion is shown in Figure 7. Observe that the final stress wave generated by the electron burst is a compressive wave of one-half the amplitude and slope of the initial stress profile, followed by a mirror-image tensile wave. Under elastic conditions, this stress wave will propagate through the absorber unperturbed until an interface is encountered.

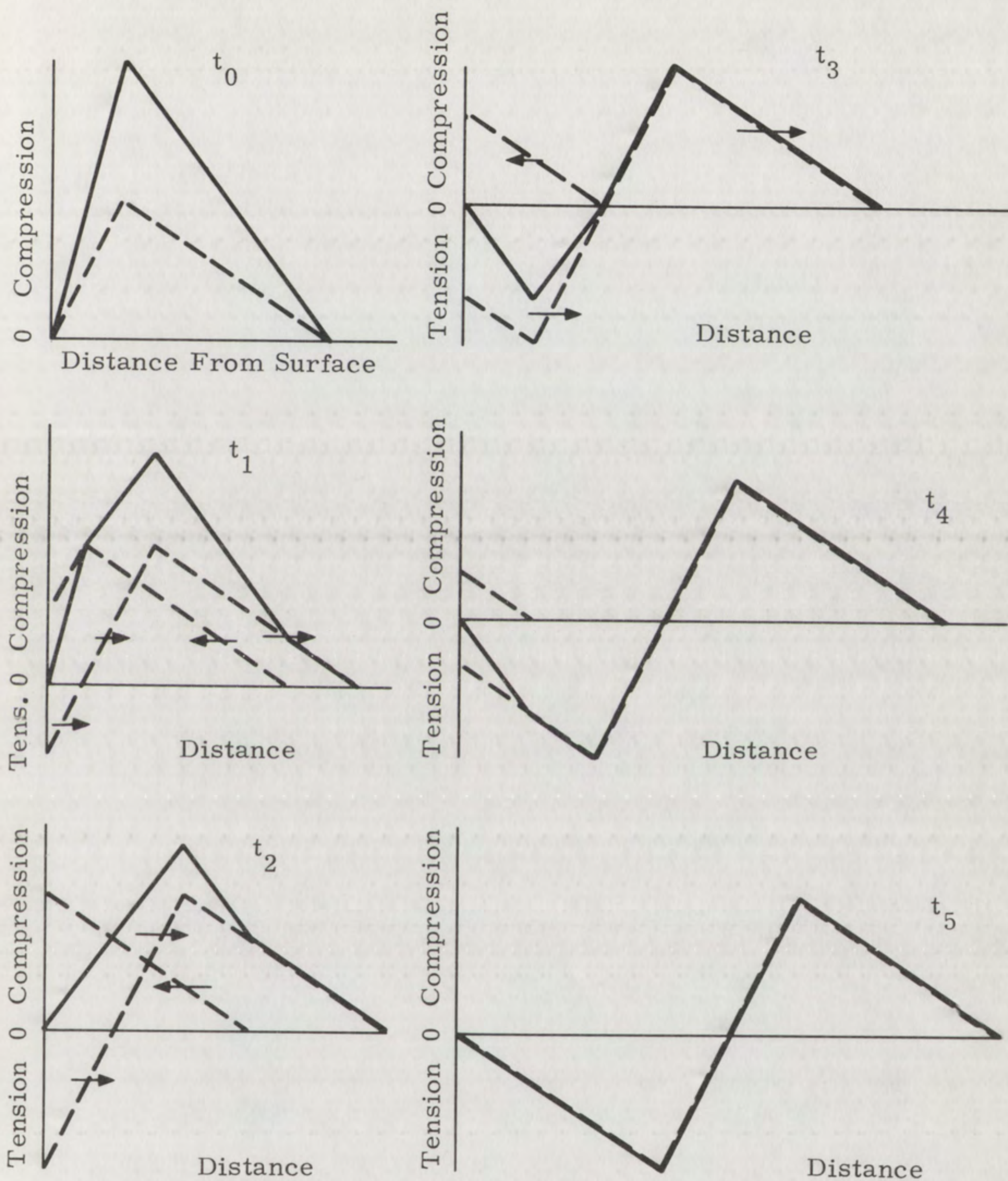

FIGURE 7.
Stress Propagation After Electron Deposition.

Throughout the foregoing theoretical development we have restricted ourselves to elastic conditions, which lead to straightforward solutions, in order to gain insight into the relations between material properties and stress-wave propagation. In any study of fracture, however, we must consider the behavior of materials that are stressed beyond their elastic limits to a condition in which strain bears a nonlinear relationship to stress. Although the insight gained in the above elastic analysis will serve us well in making qualitative judgments in all cases, precise quantitative analysis of high-pressure events will require the use of a stress-wave-analyzing computer program.

Experimental Technique

Description of Method

Thick quartz gauges have long been used to measure the stress behavior of dynamically loaded materials.[5] By placing a disc of X-cut quartz against the back surface of the material, it is possible to obtain a continuous measurement of the stress-time profile at the specimen-to-quartz interface by measuring the short-circuit current that flows

---

[5] Jones, O. E.; Neilson, F. W.; and Benedick, W. B., "Dynamic Yield Behavior of Explosively Loaded Metals Determined by a Quartz Transducer Technique," Journal of Applied Physics, V. 33, No. 11, 3224-3232, November 1962.

between the quartz disc surfaces. While the object of such measurements is usually to determine material responses to high-strain and high-strain-rate conditions, Graham[6, 7] has extended this work to develop a technique for performing electron pulse dosimetry by measuring the radiation-induced stress waves. Recall that the shape of the induced stress wave in a given material can be determined if the energy spectrum and fluence of the electron burst are known. The converse, also true, forms the basis of Graham's work. The method used in the experiments, to be described, for creating spall-inducing stress waves in transistors is an extension of Graham's technique, wherein the quartz gauge is replaced by the transistor to be exercised. By placing the transistor in intimate contact with the rear surface of the electron absorber, the same stress that was experienced by the quartz gauge will be transmitted into the transistor, subject to the known perturbations caused by the acoustical mismatch of the two materials at the interface.

A particularly interesting stress wave observed by Graham was that generated by a burst of 1.6 MeV electrons from a Field Emission

---

[6] Graham, R. A.; Neilson, F. W.; and Benedick, W. B., "Piezoelectric Current from Shock-Loaded Quartz - A Submicrosecond Stress Gauge," Journal of Applied Physics, V. 36, No. 5, 1775-1783, May 1965.

[7] Graham, R. A., and Hutchison, R. E., "Thermoelastic Stress Pulses Resulting from Pulsed Electron Beams," Applied Physics Letters, V. 11, No. 2, 15 July 1967.

Corporation Febetron 705 into an alloy 6061 T6 aluminum absorber. Figure 8 shows the stress-time profile, measured by the quartz gauge, which can be converted to a stress-distance profile in the absorber by multiplying the time axis by the shock velocity in aluminum. To determine the tensile stress that this stress wave will create at a transistor header-die interface, we recall that its magnitude will be twice that of the compression wave at the same distance from its stress node as the header-die interface from the free surface. (We establish later in our analysis that this stress will be reinforced by an equivalent tensile

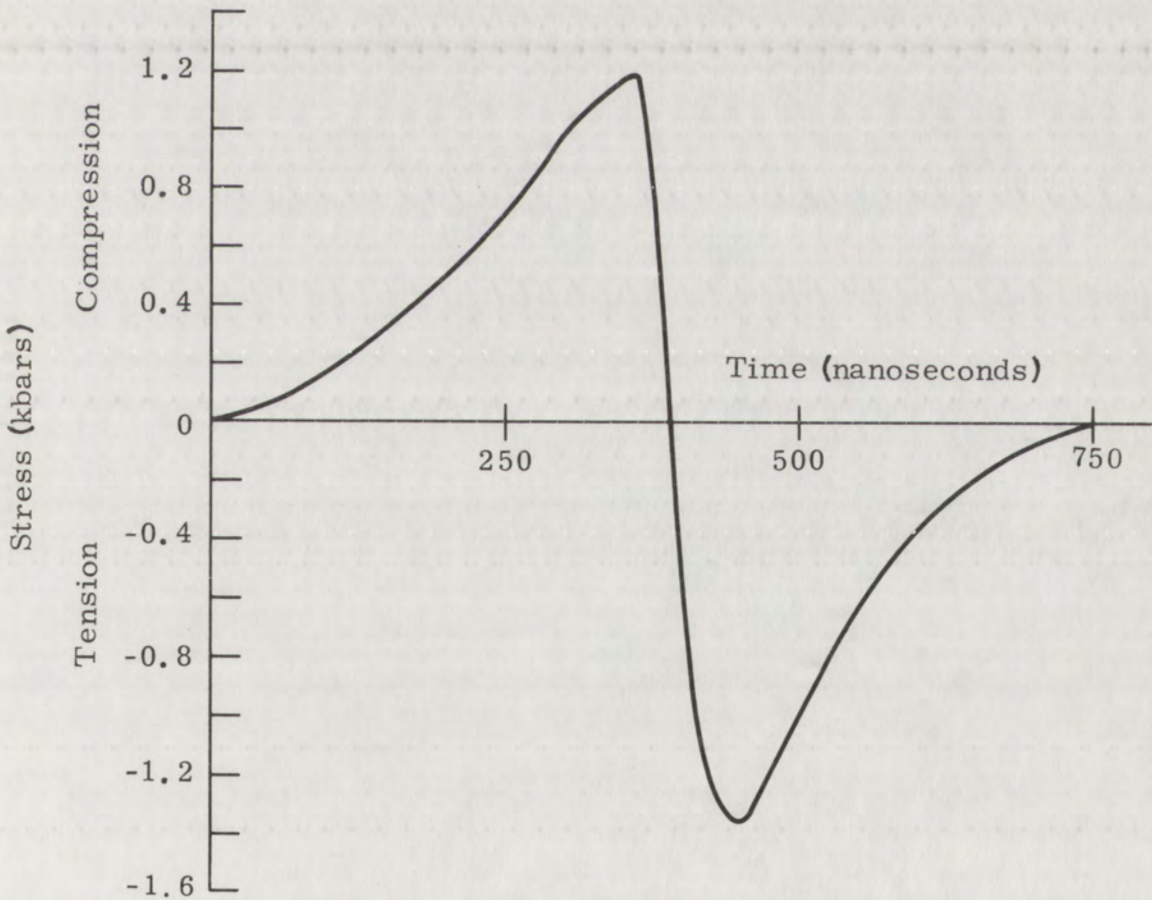

FIGURE 8.
Stress Wave Produced by Febetron 705 in Aluminum

stress from the trailing tensile wave in Figure 8 to double the tensile stress that we predict here.) A typical transistor has a die thickness of about 0.005 inch, which corresponds to a shock propagation time of about 15 nanoseconds in silicon. The compressive stress in Figure 8 at 15 nanoseconds from the node is about 700 bars; therefore, the header-die interface should experience a tensile stress of about 1.6 kbars. The actual stress will be slightly less than this because of the acoustical mismatch between the aluminum absorber, Kovar header, and silicon die.

The bond between a transistor die and header is usually considered adequate if the device survives a constant acceleration of 30,000 g. For a 0.005 x 0.020 x 0.020-inch silicon die, this acceleration would create a tensile stress at the die-attach interface of about 0.9 bar. Even considering the fact that most materials are stronger under high-strain-rate loadings, it appeared that our stress wave was capable of tensile loadings much larger than transistors have heretofore been expected to survive. In order to verify the capability experimentally, a sample of 80 transistors representative of 10 manufacturers was exposed to this stress pulse using the apparatus shown in cross section in Figure 9. The external leads were removed from the transistors, and their header bases were lapped to provide an intimate fit to the back surface of the absorber. After the lids were removed and the devices inspected, they were clamped to the absorber with a

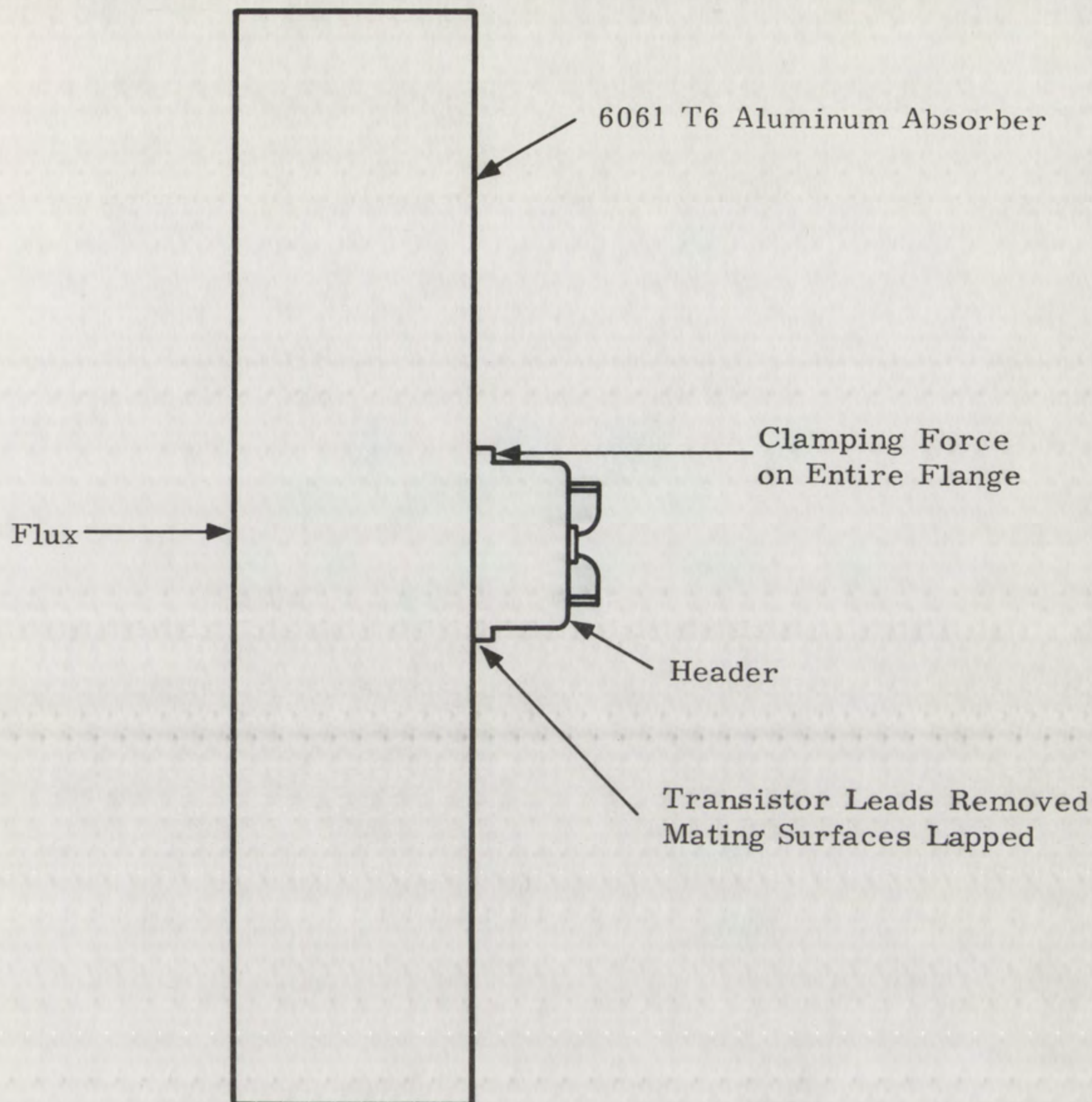

FIGURE 9.
Cross Section of Transistor Mounting Assembly.

pressure of 1 kbar at the header flange. This assembly was then mounted on a three-axis micropositioner that facilitated alignment with the electron beam axis and permitted absorbed fluence adjustments through variations in distance of the absorber from the electron tube face. A similar fixture was used to hold and position an array of calorimeters for mapping the contour and fluence of the beam before each shot.

Stress-wave configuration was then determined from previously obtained quartz gauge data relating stress profiles for the chosen absorber and electron beam to the beam fluence.

Surface doses in the aluminum absorber were varied from 7.2 to 23.7 cal/gm by varying the distance of the absorber from the tube face. It was necessary to determine the beam fluence and cross section, as well as the pulse repeatability, after each distance change by firing several bursts into an array of calorimeters arranged in a 1-1/2-inch circle, with a calorimeter at the center for fluence measurement. The fixture holding the calorimeters was designed to align the test transistor axis with the beam axis after the calorimeter array was replaced by the absorber-transistor assembly. Stress profiles in the aluminum were then determined from quartz gauge measurements performed at the same fluences measured by the calorimeters.

Experimental Results

The small sample used precluded any statistically significant failure data on the particular transistors tested; however, as a study of the feasibility of using this technique to create spall failures in transistors, the experiment was a success. Failures were created in nine out of the ten types tested and were manifested in the following manner:

1. Die-Attach Failure. This type of failure is characterized by a clean separation of the die, or portions of the die, from

the header and is believed to be due to a spall in the material, usually a thin layer of gold-silicon eutectic alloy, that cements the die to the header. Die-attach failure seems more predominant in devices using a minimal amount of the alloy. Figure 10 is a photomacrograph of a typical failure of this type. Observe that the die has become inverted by the separation process process and that the thin gold film deposited onto the bottom of the die before attachment remains intact.

2. <u>Die Spall</u>. This type of failure, more common to devices using relatively large amounts of gold-silicon alloy (often in the form of fusible preforms), is the brittle fracture of the silicon die in a plane parallel to and slightly displaced from the plane of attachment. Figure 11 shows an example of this phenomena, where most of the die has been spalled out of the picture, but some of it remains suspended above the header by the emitter and base leads.

3. <u>Die Fracture</u>. This type of fracture is characterized by one or more vertical fractures of the silicon die and may or may not involve separation of the resultant fragments from the header. Figure 12 shows an example of simple die fracture where the largest fragment has separated and is suspended above the header by the emitter and base leads.

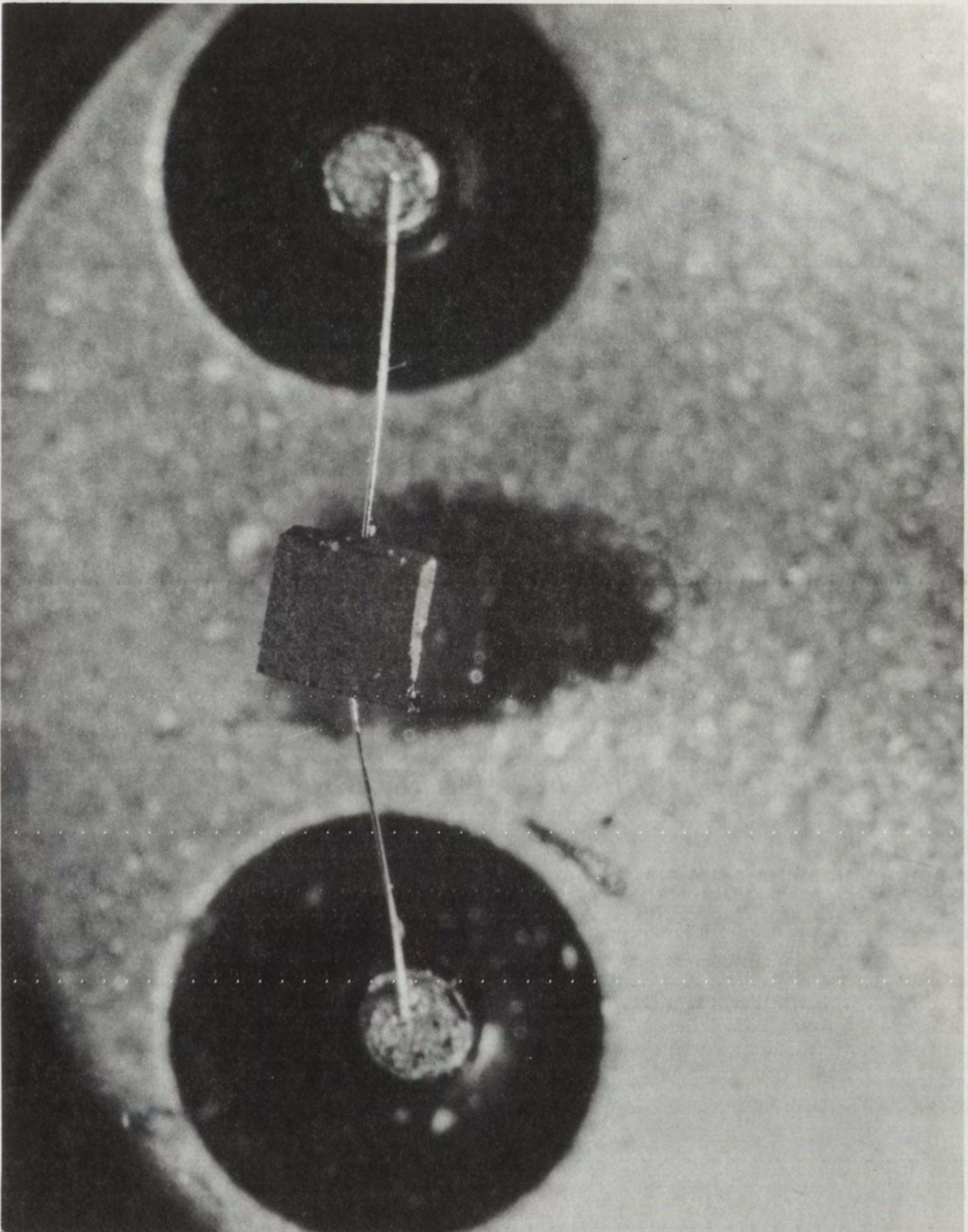

FIGURE 10.
Typical Die-Attach Failure.

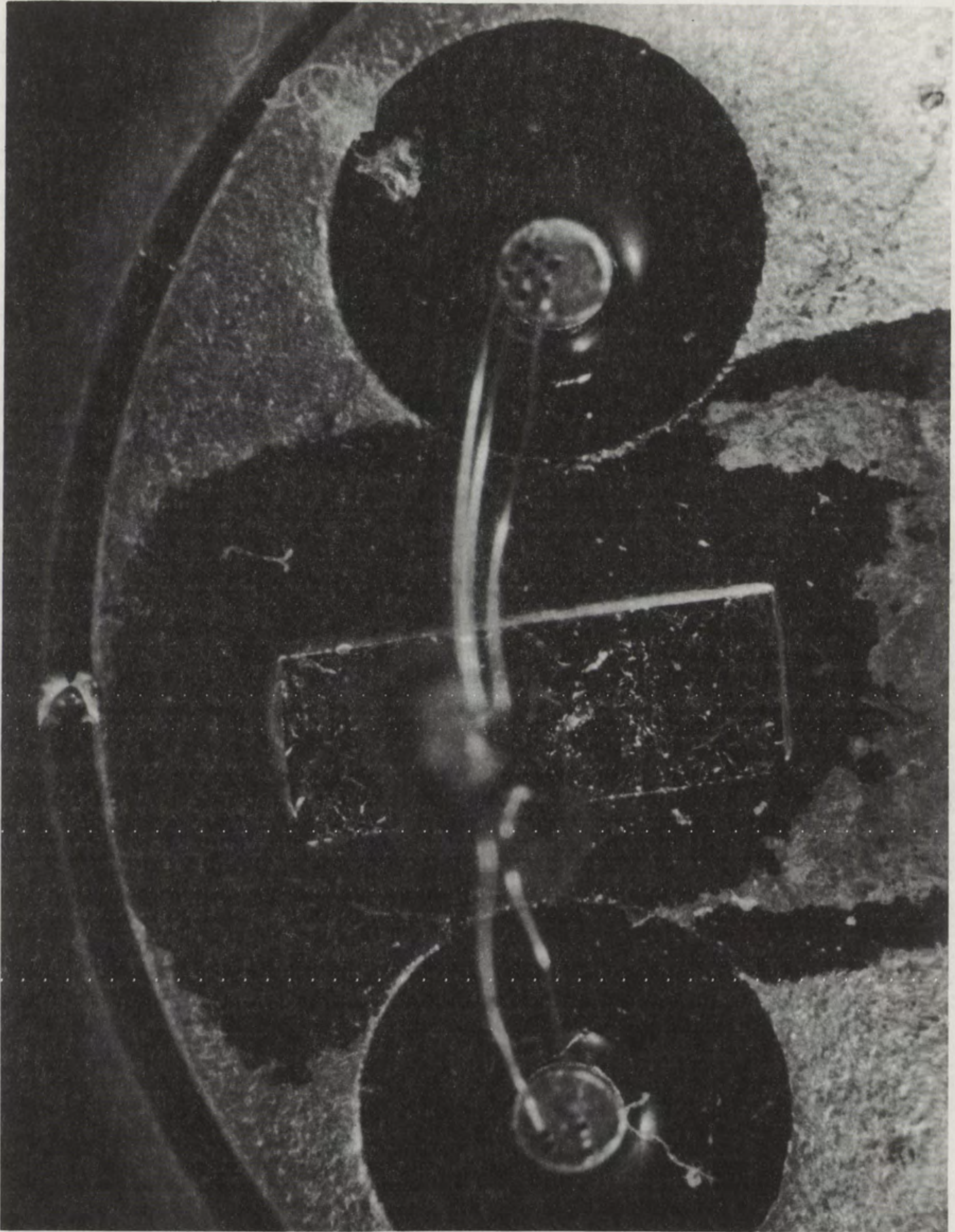

FIGURE 11.
Typical Silicon-Die Spall.

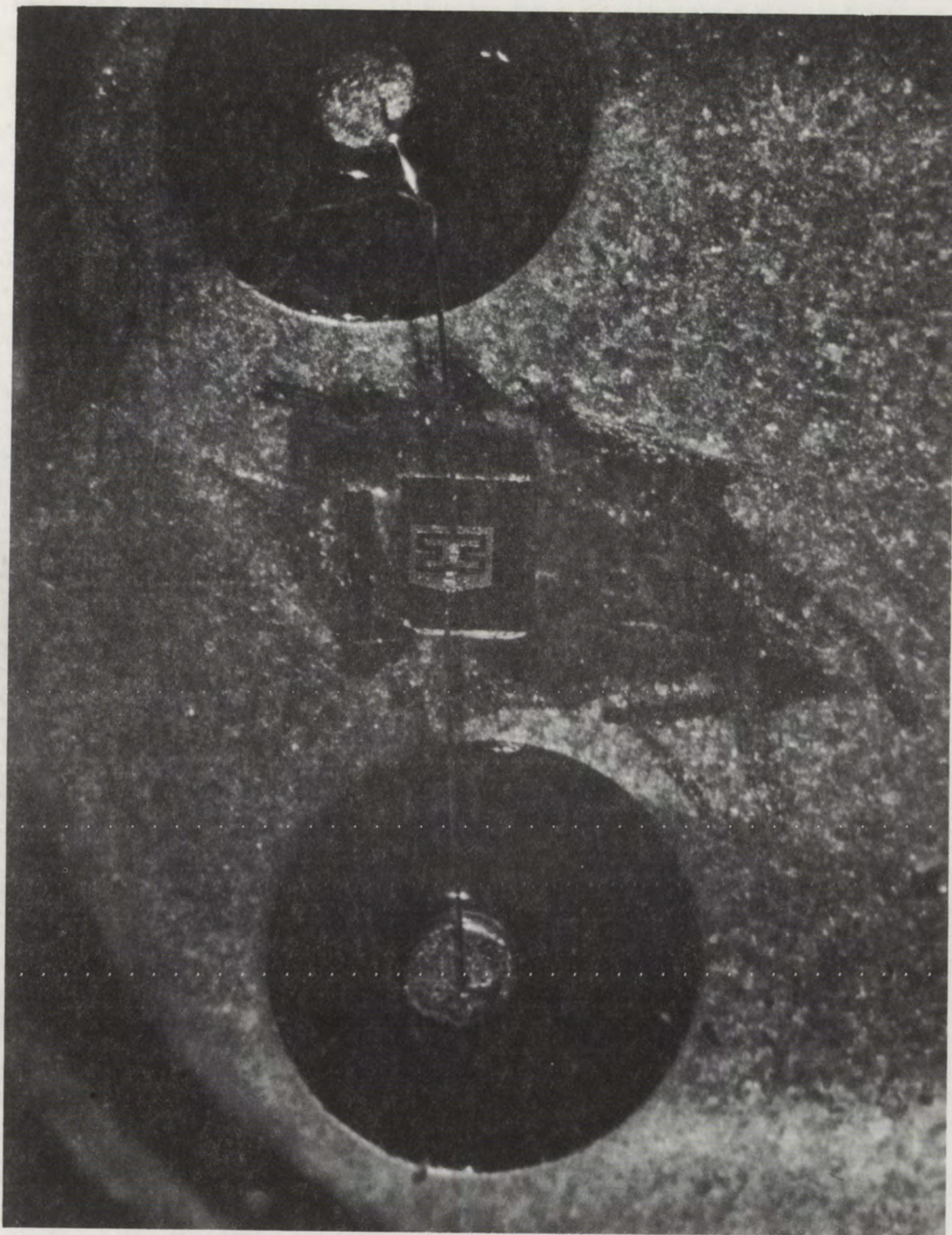

FIGURE 12.
Typical Die Fracture.

4. Wire-Die Bond Rupture. This type of failure, usually limited to stresses below those required for die attach or die spall and to devices using aluminum leads and metallization, is a rupture of the bond between an emitter or base leads and its corresponding metallization on the die. Figure 13 shows an example of this where one of the three emitter leads has become detached. Note that die spall has also occurred.

5. Wire-Post Bond Rupture. This type of failure, limited to lower stresses, is a rupture of the weld between either the base or emitter leads to their respective posts, which are the internal protrusions of the external leads that enter the device through Kovar-glass seals. Details of a typical wire-post bond rupture are shown in Figure 14.

6. Compound Failures. A combination of the above failures is often observed at the higher stress levels. Figure 15 shows an example of die-attach spall, die fracture, and wire-die bond rupture, but survival of the wire-post bond. The stress levels responsible for each failure are difficult to analyze, as we shall see later, because the sequence of failure events is not usually obvious.

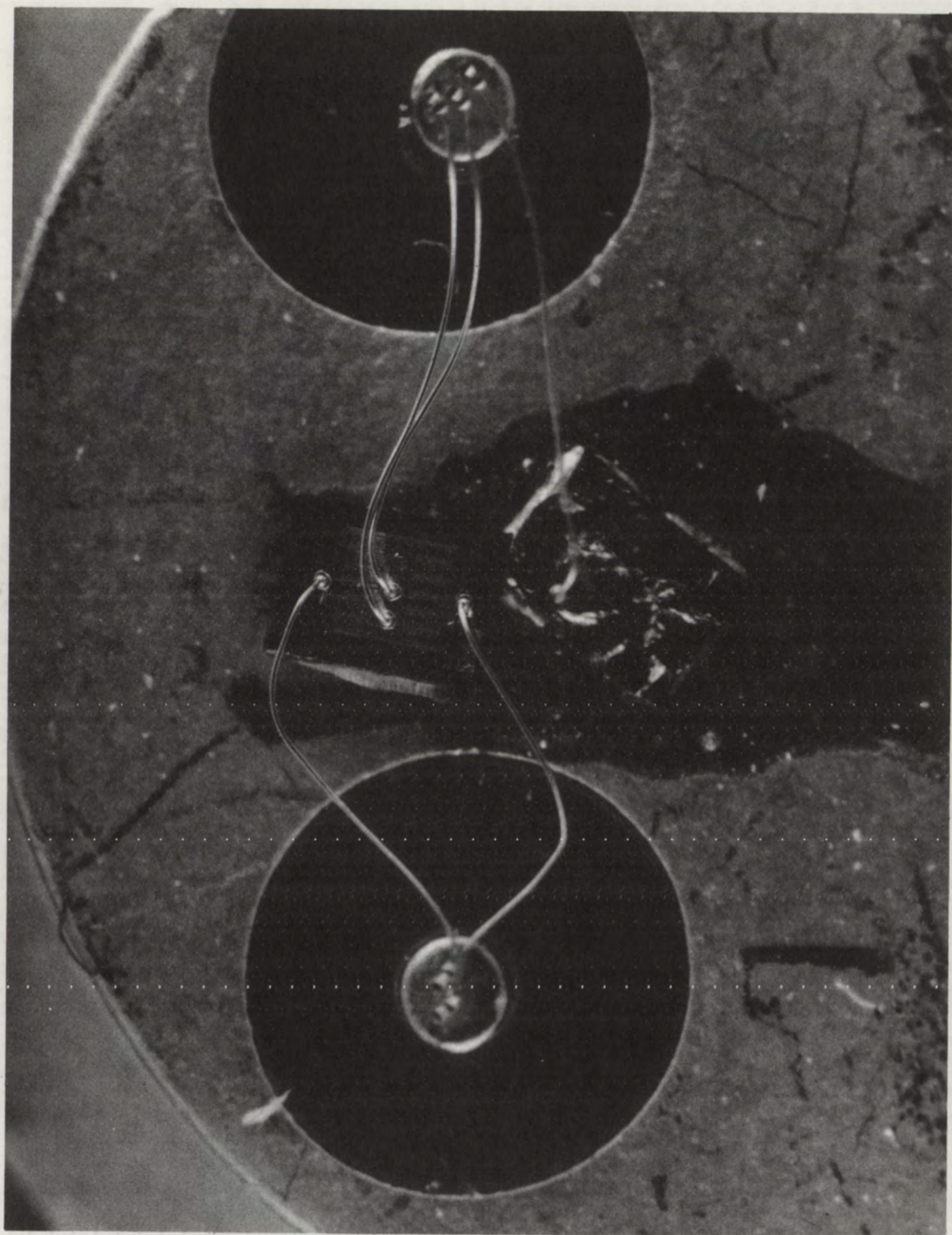

FIGURE 13.
Wire-Die Bond Rupture.

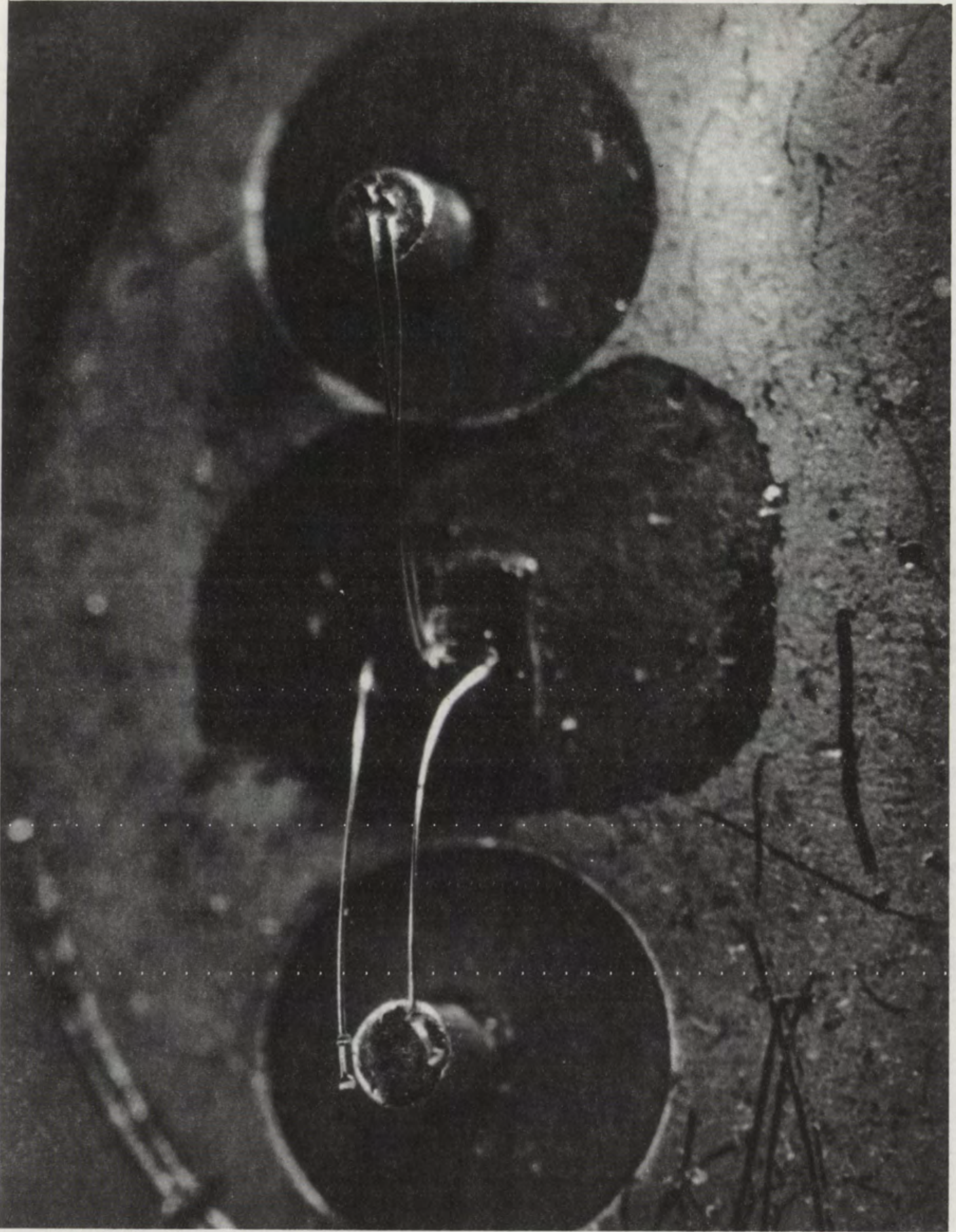

FIGURE 14.
Typical Wire-Post Bond Rupture.

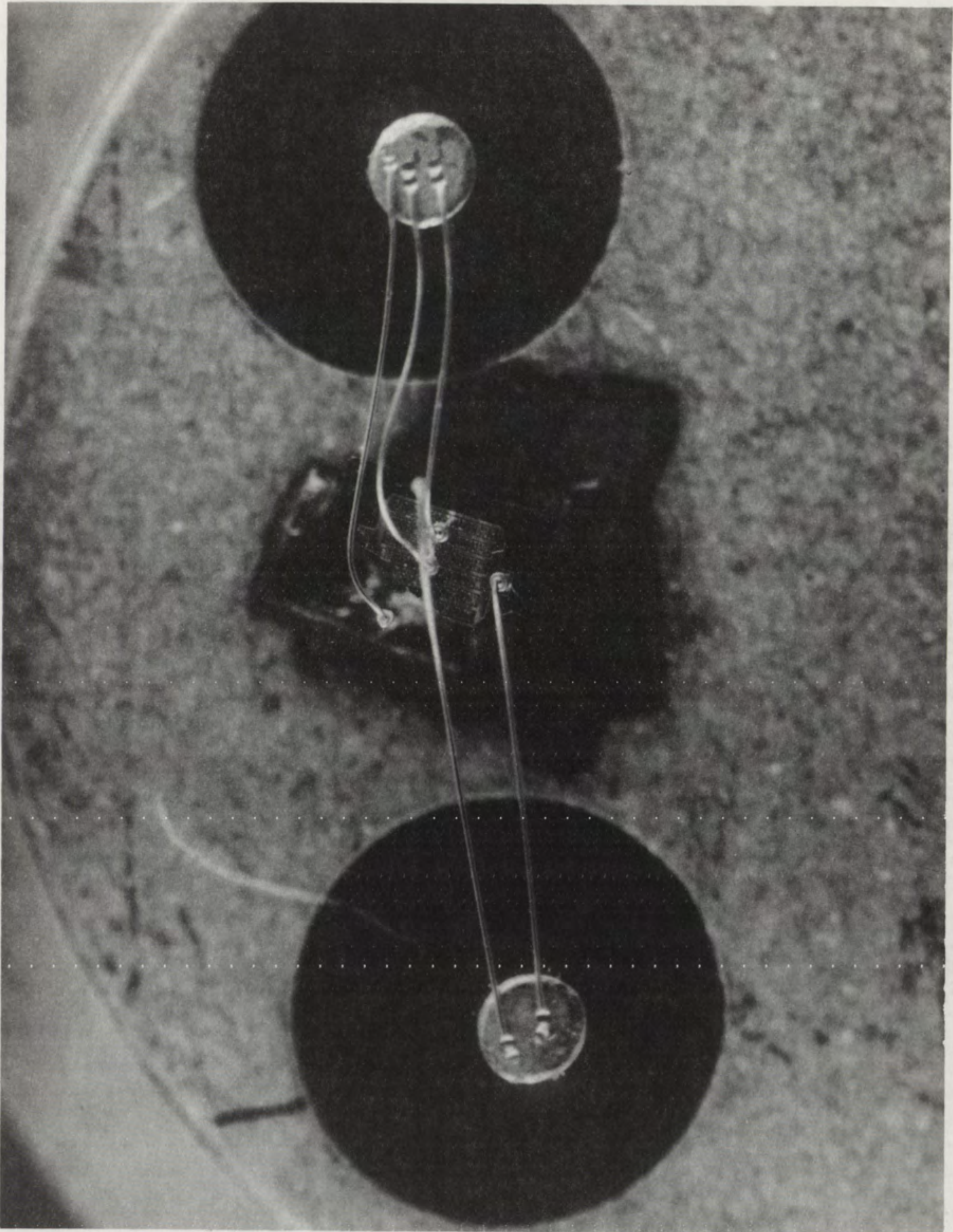

FIGURE 15.
Example of Compound Failure.

It should be reemphasized that the experiment described here was not intended to determine precise failure levels of the devices investigated, but to establish that the technique devised could produce sufficiently high stress levels of adequate resolution to cause a complete range of failure mechanisms. Precision was precluded not only by the small size of the sample, but also by errors introduced by nonsimultaneous dosimetry or quartz gauging and imperfect fixturing. The data obtained are, however, adequate to demonstrate the analytical technique described in the following section.

Analysis

In order to relate the observed failures to some failure criteria associated with the stress history that prevailed at the location of failure, it is necessary to: (1) formulate a model to which predicted requirements of failure can be ascribed, (2) calculate the stress response of this model to the known stress inputs, and (3) adjust the model parameters until the analysis is capable of predicting all of the results that were observed. The model chosen here was a unidimensional-strain cross section through the axis of symmetry of the transistor (normal to the header). The condition of failure was assumed to be a tensile stress that exceeded the ultimate dynamic yield of the interface that spalled. Although the results of this approach did not completely describe all observations, the analytical technique is sufficiently

general that it can be used to incorporate more sophisticated constraints, such as time-dependent failure criteria, that will ultimately result in adequate correlation. The approach is presented here to show the inseparability of experiment and analysis in the formulation of a technique for predicting the survival of transistors to a general stress-wave input.

Because of the prohibitive number of calculations necessary to determine the response of a transistor to a stress wave that exercises some of the composite materials into their inelastic regions, most calculations referred to in this report were performed on the CDC 3600 computer, using the SWAP-7[8] elastic-plastic stress-wave-analyzing program. The function of this code is to calculate the many shock, interface, and free-surface interactions that occur in a shock-loaded structure and to output the results in the form of stress profiles throughout the structure as a function of time.[9] Because the code is limited to stress profiles along a single dimension, it was adapted to our study by choosing a unidimensional cross section through the transistor wire-die bond, silicon die, gold die-attach, Kovar header, and aluminum absorber in a direction normal to the surface of the die. The program was initiated by analytically moving the stress wave,

---

[8] Barker, L. M., SWAP-7: A Stress-Wave Analyzing Program, Sandia Corporation Report SC-RR-67-143, April 1967

[9] See Appendix B for more details on SWAP-7

measured by the quartz gauge at the rear surface of the absorber and approximated by a series of shock waves, back into a position in the absorber so that the leading edge of the stress wave is nearly incident on the interface between the absorber and the transistor header. This initial shock position and the single-dimension cross section of a typical transistor is shown in Figure 16. At this point, the computer is turned on and the stress wave is propagated into the transistor.

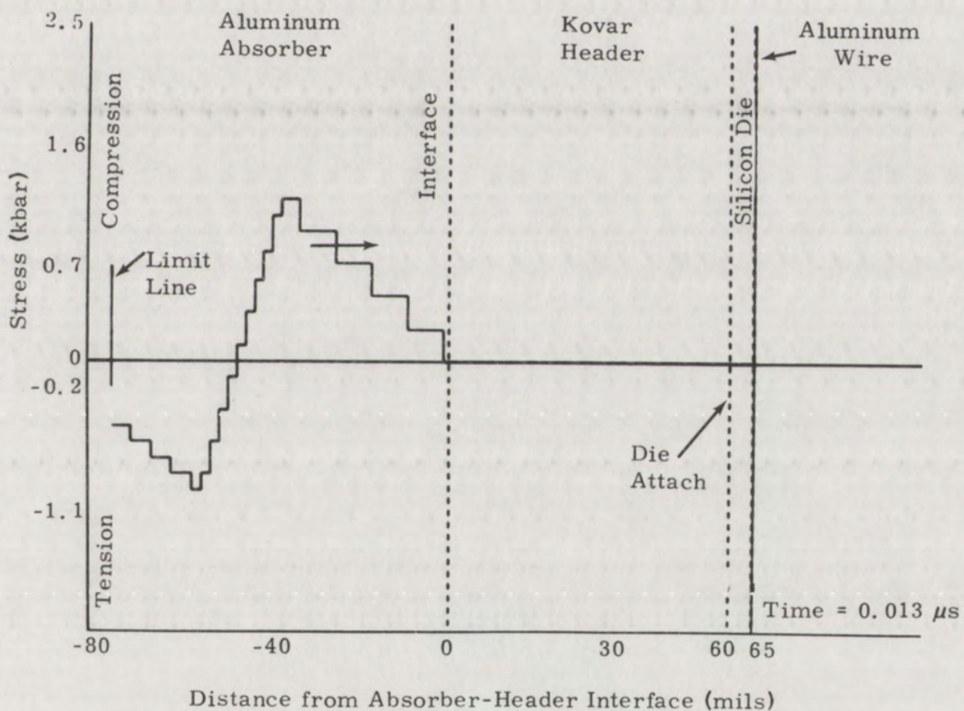

FIGURE 16.
Initial Conditions of SWAP-7 Computer Run.

The transmission coefficient for the aluminum-Kovar interface is 1.47 and the reflection coefficient is 0.47. This means that after traversing the interface the stress-wave amplitude will be 47 percent greater and, at some point during transmission, the peak tensile at the interface will also be 47 percent greater than that of the incident wave. Figure 17 shows both these effects at 235 nanoseconds after the stress wave first reached the interface. However, stress amplification may be only temporary for, at subsequent interfaces, the reverse process may prevail and the net result will be only an energy loss due to the

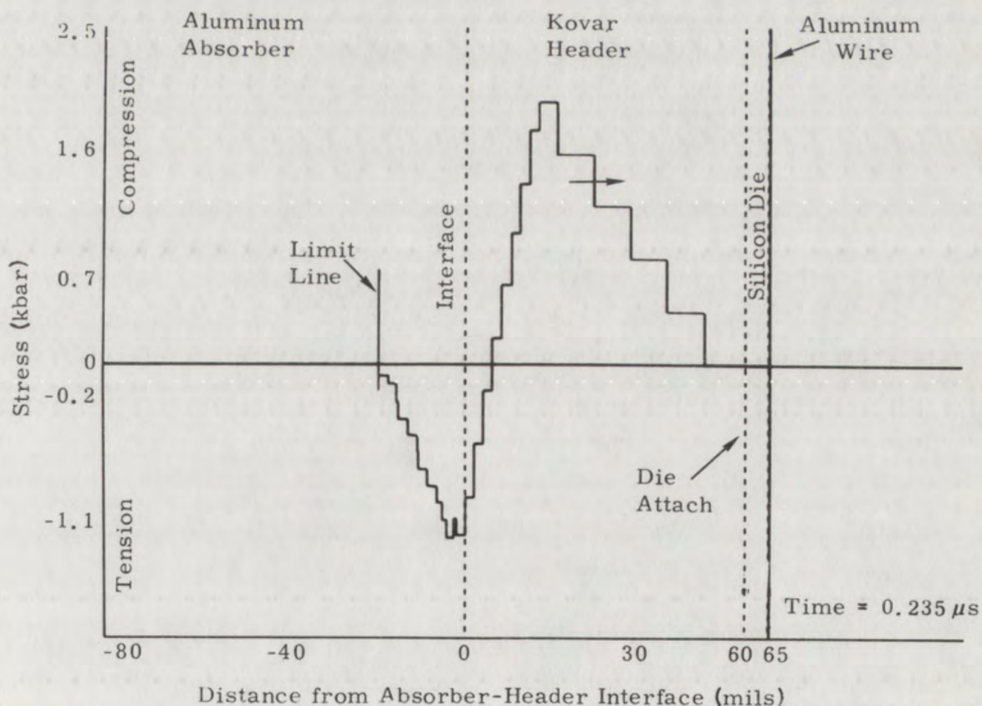

FIGURE 17.
Stress Amplification by Impedance Mismatch.

reflections at both interfaces, with no net change in stress levels. Tensile amplification at the interface, however, may be important if the separation stress is reached, which is the case in the present example where the 1-kbar clamping pressure is exceeded. Figure 18 shows that, at 236 nanoseconds, separation of the header from the absorber occurs (indicated by the computer by a solid heavy line). Until the separated surfaces are again forced together by subsequent stress waves, no further stresses can be transmitted across the interface.

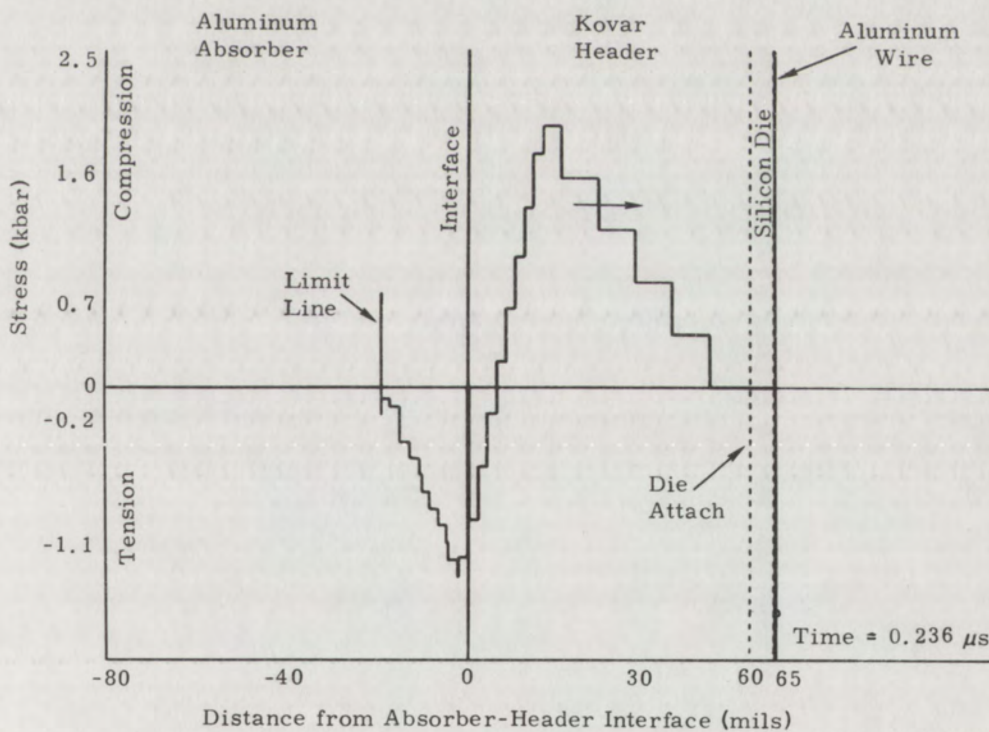

FIGURE 18.
Absorber-Header Interface Separation.

The stress-wave truncation, which is more apparent in Figure 19, does not lessen the damaging effects of this rather long pulse but may be of serious concern when shorter stress waves are used. The limit line shown in these figures was introduced into the program to eliminate all left-moving shocks, such as the reflected truncated section, that are no longer of interest but can increase computation time and overload the computer memory.

When the leading edge of the stress wave reaches the free surface of the aluminum lead wire, tensile waves of amplitude equal to the

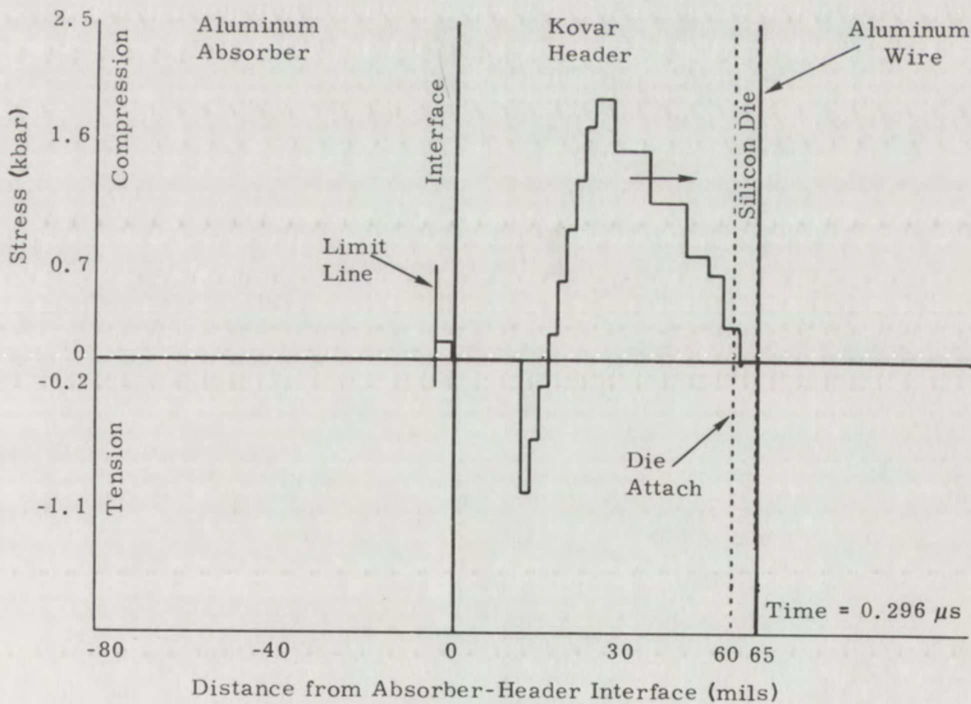

FIGURE 19.
Reflections from Free Surface Begin

oncoming shocks are reflected and temporarily reduce the stress near the surface to almost zero, as shown in Figure 19. Until the compressive peak reaches the surface, the incident shocks are always about the same amplitude as the corresponding tensile reflections, so stresses in the transistor region remain low during this period. However, after the compressive peak reflects, subsequent incident stress changes are tensile as the wave rapidly decreases to a state of tension (see Figure 19). For the example chosen, which is typical of all devices studied in this

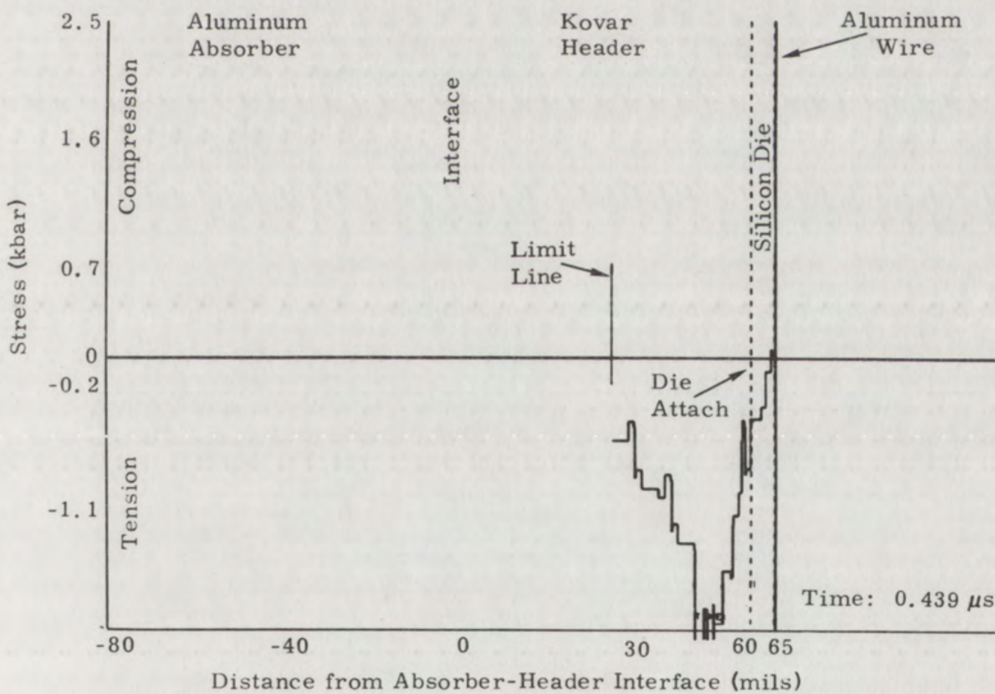

FIGURE 20.
Tensile Reinforcement Near Free Surface.

experiment, these incident tensile shocks appear in the transistor region at the same time as the tensile reflections from the immediately preceding compressive shocks. The results of this tensile reinforcement are shown in Figure 20, where the stresses in the die and die attach are considerably greater than would be expected from the incidence of only the tensile portion of the original stress wave. This magnified tensile condition, which actually exceeds the ordinate scale limits, continues as long as tensile reflections are in the vicinity of the incident tensile wave and may exceed the spall threshold at some point in the device, as indicated in Figure 21.

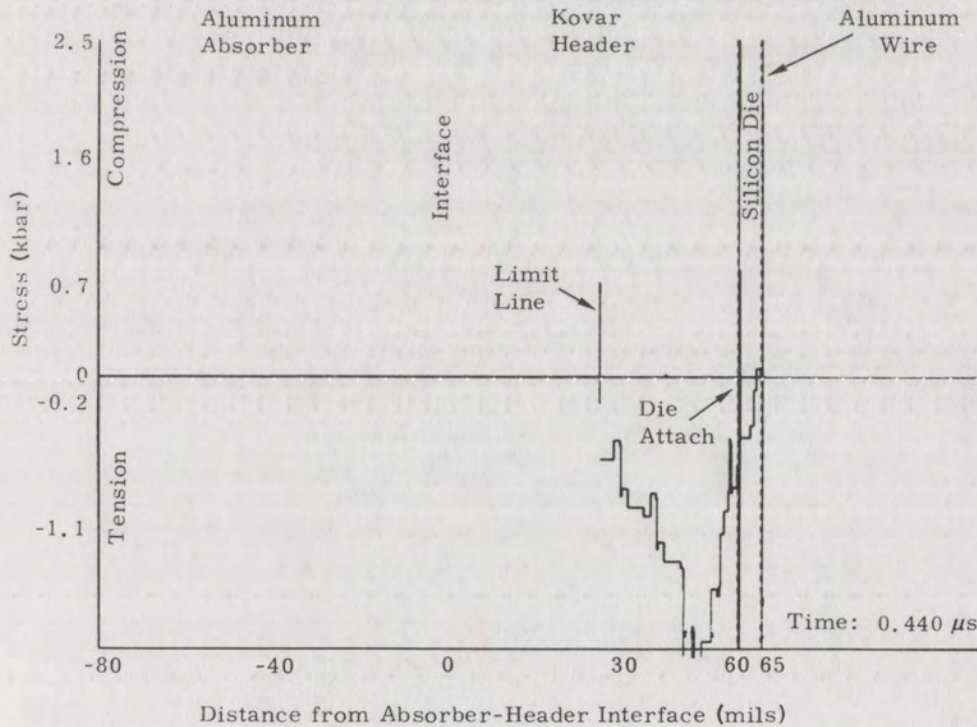

FIGURE 21.
Die-Attach Spall.

At 440 nanoseconds after stress-wave incidence on the header base, the computer has indicated that the spall threshold of the die attach has been exceeded. From this point on, no further energy can be transmitted to the die, so the stress trapped therein merely rings between the free surfaces, unable to cause further damage. This condition is shown in Figure 22. It is interesting to note that at a slightly lower incident stress, not quite sufficient to cause die-attach spall, enough energy might have been transmitted through the intact die attach

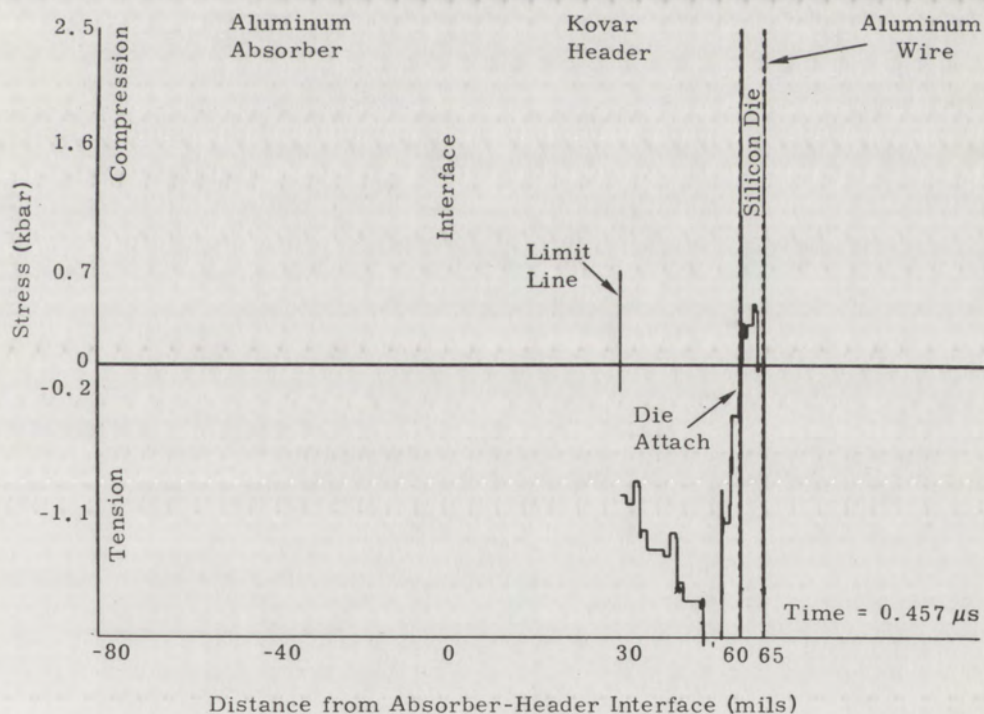

FIGURE 22.
Stress Ringing in Separated Die.

to have caused wire-die bond separation. This complex time-dependency of failure emphasizes the need for a computer code, such as SWAP-7, that can account for perturbations caused by material failures.

Calculations were performed for each transistor type by first using the stress pulse that was found to cause the initially observed failure. By suppressing failure in this initial calculation and observing the maximum tensile stress that appeared at the point of failure, it was possible to determine the tensile stress necessary to cause spall, which was the ultimate goal of this study. Should subsequent calculations become necessary (for example, to determine the effects of higher doses that were found to cause compound failure modes), the perturbations of the stress wave caused by the initially observed failure can be accounted for by the computer if the now-known spall thresholds are included with the input data and if separation is no longer suppressed by the program.

Table 1 is a summary of the results obtained using this technique. Spall thresholds are shown wherever possible, and survival levels are indicated for devices that either did not fail under the highest fluence levels used or that exhibited compound failures in such a manner that sequence of failure could not be established with confidence. Solution of the latter uncertainty is being attempted, at present, by the use of high-speed photography to observe the sequence of events leading to

Table 1

SUMMARY OF RESULTS

Transistor Type	Die Attach		Die		Wire-Die Bond		Wire-Post Bond	
	Fail (kbar)	Survive (kbar)	Spall (kbar)	Survive (kbar)	Fail (kbar)	Survive (kbar)	Fail (kbar)	Survive (kbar)
2N2369A	0.66			0.44	0.15		NA*	NA*
2N2729		1.0	0.75			0.31		0.56
2N3553 Type 1	0.72		0.49			0.33		0.72
2N3553 Type 2		0.5	0.32			0.13		0.88
2N3553 Type 3		0.88	0.38		0.36		0.19	
NS9726		0.82	0.51			0.21	NA	NA
2N3886		1.06	0.75			0.34	0.18	
ST6164		0.65		0.40		0.18		0.19
TIXS39		0.94		0.75		0.25	NA	NA
ST2120	0.38		0.54			0.22	0.38	

*Analysis not applicable

failure, an example of which is the simultaneous rupture of the die attachment and wire-die bond. Post-mortem analysis is not sufficient to establish whether the wire bond failed by shock-wave interaction or by a tensile force created by the momentum of the die being propelled away from the header. Preliminary photographs indicate that the latter condition is the most prevalent.

In addition to determining the spall thresholds that are vital to the theoretical prediction of the device response to particular stress waves, it is useful to those engaged in increasing device tolerance of these environments to study the effects of device geometry on the stress waves. The reinforcement of tensile relief waves originating at the die free surface with the tensile contribution from the incident stress wave usually occurs in the region most susceptible to tensile failure. Several modifications to the device structure that would alleviate this condition are suggested by these stress interactions: (1) increasing the tensile strengths of this region by improvements in fabrication or (2) extending the free surface of the structure so that tensile reinforcement will occur in less strategic locations. The former could be accomplished by improved die-attachment techniques and by forming dice from the parent wafers in such a way as to eliminate the fracture nucleation sites created at the dice peripheries by present dicing techniques. The free surface of the die could be extended by encapsulating the interior of the device.

Conclusions

The technique described above for determining the spall strengths of transistors is a quasiempirical approach that requires an iterative blending of experimental and analytical procedures. To the extent of establishing that the experimental procedure will produce the desired

stress response and that the analytical procedure is capable of deriving consistent and quantitative information from the experiment, the work described herein was successful. Specimens from nine out of ten classes of transistors were damaged in an orderly manner which suggested not only that certain types of failure are dependent on fabrication details but also that the laboratory procedure was sufficiently controlled that the dependencies were not obscured by experimental error. Analysis based on the assumption that spall is a time-independent result of exceeding a given tensile threshold yields consistent results, but is not sufficiently sophisticated to provide a precise description of the sequence of events leading to failure. Independent failure-time measurements indicate that, in general, failure occurs after longer periods of elapsed time than those predicted by the method described in this report. This indication suggests a stress-time dependence that may be better correlated by using total stress energy as the parameter. Because this technique is sufficiently versatile to permit a choice of failure criteria, it was concluded that within the limits of this technique the capability existed for determining the spall thresholds of present-generation transistors and, with a reasonable extension, that even the more robust next-generation devices could be characterized.

Future effort will be directed toward increasing the consistency and precision of this technique with the ultimate goals of (1) a precise definition of the cause of failure in transistors and the most sensitive

parameters associated with it and (2) an extension of the technique to include studies on other classes of electronic components. In order to separate the relative effects of stress, time, and geometry on failure, it is necessary to be able to vary both stress signature and analytical model. The former can be accomplished by using various absorber materials and electron-accelerating voltages or a laser photon source and selected optical-density absorbers. Variations in the analytical model will be necessary to accommodate controlled changes in device geometry and will consist mostly in matching the stress-wave-analyzing code to the restrictions imposed by geometry and stress signature. For example, should unidimensional strain conditions fail to hold, a two-dimensional code, such as TOODY,[10] can be used to account for the effects of shear waves.

---

[10] Thorne, B. J., and Herrmann, W., TOODY A Computer Program for Calculating Problems of Motion in Two Dimensions, Sandia Corporation Report SC-RR-66-602, July 1967.

APPENDIX A

FLYER-PLATE LOADING DISADVANTAGES

The response of semiconductor devices to stress waves becomes difficult to analyze if momentum is imparted to the devices during the loading process. In the case of transistors loaded with explosively accelerated flyer plates, this momentum can cause spurious stresses at the wire-die bonds of such magnitude that spall is completely masked. It is the purpose of this appendix to demonstrate how these stresses arise.

Consider the simplified cross section of a transistor shown in Figure 23. Using exploding-foil techniques, it is possible to impact a Mylar flyer plate onto the bottom of the Kovar header with a velocity of 5 mm/μsec. Using the material properties shown in Table 2, one can generate the distance-time (x-t) plot shown in Figure 24.

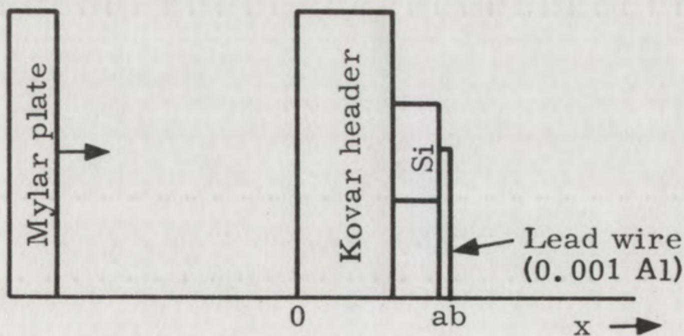

FIGURE 23.
Cross Section of Idealized Transistor.

Table 2

PROPERTIES INFLUENCING STRESS RESPONSE

Property	Mylar	Kovar	(111) Silicon	Aluminum
	Material			
Density, ρ (gm/cm^3)	1.4	7.9	2.33	2.72
Shock Velocity, U_s (mm/μsec)	2.9	4.2	9.36	5
Impedance, I $\left(\frac{kbar/\mu sec}{mm}\right)$	40	332	218	136

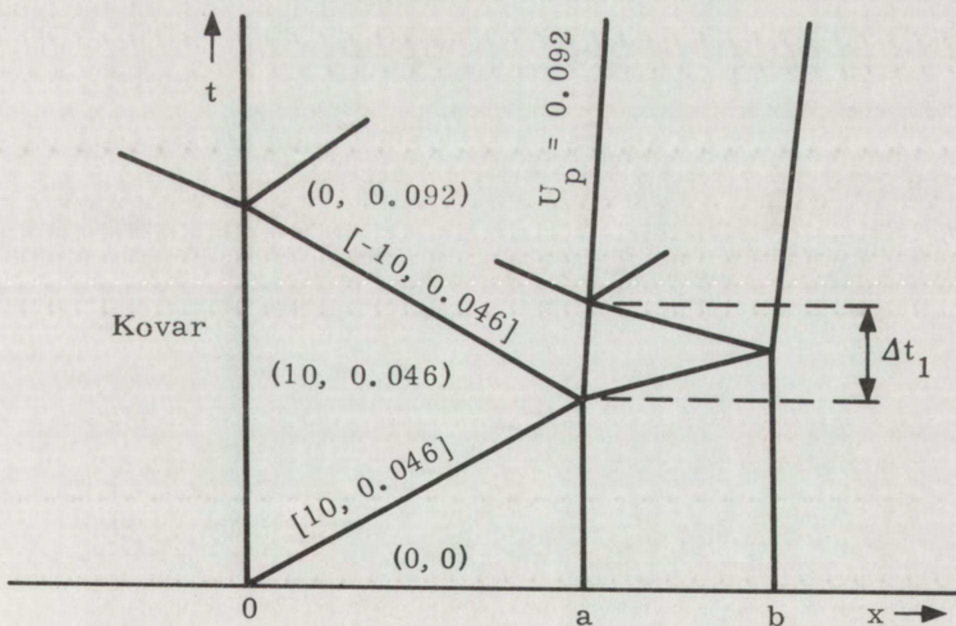

FIGURE 24.
x-t Plot for Flyer-Plate Impact.

The stress generated in the Kovar header by the impact is given by

$$\Delta\sigma_K = \frac{I_M I_K}{I_M + I_K} U_{P_M} = \frac{40(332)(5)}{40 + 332} = 178 \text{ kbars}$$

where subscripts K and M refer to Kovar and Mylar, respectively. Except for attenuation in the Kovar by rarefaction waves, this stress propagates to the Kovar-silicon interface, where the transmitted stress can be calculated as follows:

$$\Delta\sigma_S = \frac{2I_S}{I_K + I_S} \Delta\sigma_K = \frac{2(218)178}{332 + 218} = 141 \text{ kbars}$$

where subscript S refers to silicon. Again this is a worst-case condition, but indicates the possibility of at least a 10-kbar shock wave being transmitted into the silicon die. It was this assumption on which the x-t plot of Figure 24 was based.

The time interval, Δt, during which the lead wire is accelerated by the silicon surface to a velocity of 0.092 mm/μsec, is found by dividing twice its width by its shock velocity.

$$\Delta t_1 = \frac{2 \text{ x dia. (in mm)}}{U_S} = \frac{2(0.001)25.4}{5} = 0.01 \ \mu\text{sec.}$$

An "average" acceleration may be estimated by

$$\bar{a} = \frac{\Delta V}{\Delta t} = \frac{U_p}{t_1} = \frac{0.092}{0.01} = 9.2 \text{ mm}/\mu\text{sec}^2.$$

This acceleration will give rise to a shear stress in the wire of

$$\tau = \rho U_s U_p = 2.72(10)\,5\,(0.092) = 12.5 \text{ kbars.}$$

Although the dynamic shear strength of aluminum will be somewhat higher than the static yield of 1.4 kbars, one would expect the 12.5 kbars to be sufficient to cause wire rupture. An acceptable transistor wire bond will yield under a static tensile stress of about 1/3 kbar; therefore, even if the wire does not rupture, the wire bond will be destroyed by the Newton forces from the accelerated wire. It is this type of perturbation that is undesirable during spall studies.

APPENDIX B

APPLICATION OF SWAP-7 COMPUTER CODE

The SWAP-7 computer code, written for the CDC 3600, calculates the many shock, interface, and free-surface interactions that occur in a shock-loaded structure and outputs the results in the form of stress profiles throughout the structure as a function of time.

The calculation of the response of composite materials to a stress wave generated by the near-instantaneous absorption of electrons can be compared to the solution of the transient response of a complex electrical circuit by (1) following the progress of electrical currents in all branches simultaneously; (2) performing graphic solutions each time a discontinuity such as a node, a component, or a change in electrical pulse shape is encountered; and (3) maintaining a graphic record of voltage and current waveforms throughout the circuit as a function of time. Fortunately for circuit analysts, the assumption of constant component values is usually valid, forcing functions are usually easily described mathematically, and techniques have been developed for obtaining closed-form solutions to an acceptable degree of precision. Since similar treatment of stress-wave analysis on even simple systems usually yields unrealistic solutions, the circuit analyst must usually resort to an iterative, machine-performed approach such as SWAP-7.

Determination of the products of a shock-shock or shock-interface interaction presumes a knowledge of the equations of state and stress histories of the materials involved. Because these are interdependent and nonlinear, a graphic record is necessary and usually takes the form of a stress-distance and a stress-time plot. As information is accrued from graphic solutions of interactions performed with shock-velocity/particle-velocity characteristics of the materials involved, these plots grow in size and complexity until the sought-for interaction occurs. A typical solution of the response of a transistor to the stress wave described in this report would require over 10,000 graphic interaction solutions. SWAP-7, using the same general approach, performs these calculations on the CDC 3600 in about 15 minutes.

The information required by SWAP-7 for the solution of the problem described by this report consists of the (1) dimensions and equation-of-state data of all materials that lie along the selected unidimensional cross section through the transistor and electron absorber, and (2) particle velocities, strains and shock velocities of each of the shocks used to approximate the continuous stress generated in the absorber. In its present form, SWAP-7 accepts only shock-wave or instantaneous-energy-deposition forcing functions, so the approximating shock-wave parameters have to be hand calculated.

For those interested in using SWAP-7 for related applications, the following procedure for calculating these parameters is presented:

1. Approximate the stress wave by a series of shocks, as shown in Figure 25. The number of cuts is usually limited to 20 by the present form of SWAP-7.

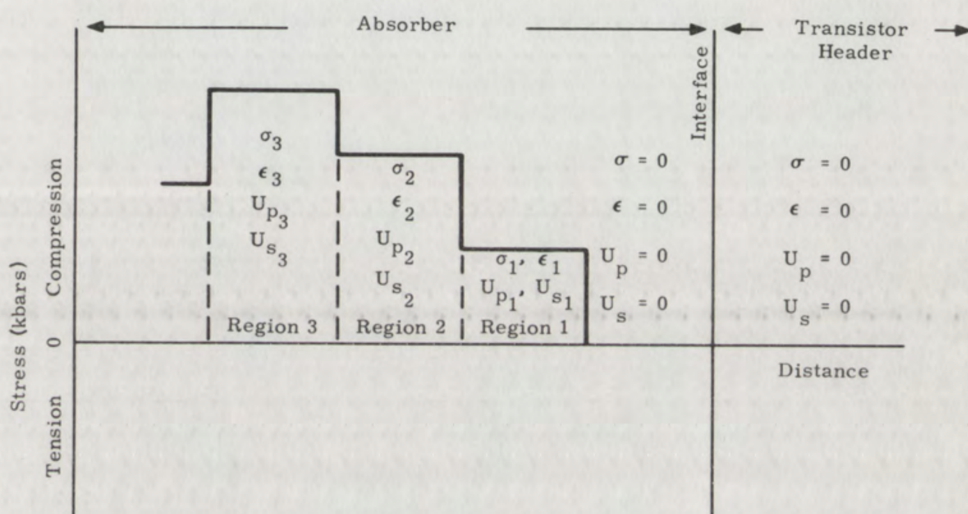

FIGURE 25.
Example of SWAP-7 Input Parameters.

2. Determine, for the chosen absorber material, the Hugoniot elastic modulus of elasticity

$$F = \frac{\partial \sigma}{\partial \epsilon} \text{ in kbars.}$$

F can be approximated, using

$$F = K\left[\frac{3(1 - \mu)}{(1 + \mu)}\right]$$

where K is the bulk modulus, and μ is Poisson's ratio.

For 6061 T6 aluminum, F = 1120 kbars.

3. Consider the stress, σ_1, in region 1 and calculate the strain

$$\epsilon_1 = \frac{\sigma_1}{F} .$$

4. Calculate

$$U_{p_1} = \frac{\sigma_1}{\sqrt{10\rho F}} \quad \text{and} \quad U_{s_1} = \sqrt{\frac{F}{10\rho}} \ \text{mm}/\mu\text{sec}$$

where U_{p_1} is the particle velocity, U_{s_1} is the shock velocity, ρ is the density, and the factor 10 is needed for dimensional consistency.

At this point, we have all parameters needed for the state cards for region 1. Because all velocities are defined relative to the material ahead, the parameters for the succeeding shock in the ith region, where $i = 1$ for region 1, are found as follows:

5. $$\epsilon_i = \frac{\sigma_i}{F} .$$

6. $$U_{p_i} = \frac{\sigma_i - \sigma_{i-1}}{\sqrt{10\rho F}} + U_{p_{i-1}} .$$

7. $$U_{s_i} = \frac{1 - \epsilon_i}{10\rho} \sqrt{10\rho F} + U_{p_i} .$$

8. Enter ϵ_i in the E(J) in the first state card for region i.
9. Enter U_{p_i} in UPA(I) and UPB(I) in the appropriate line cards associated with region i.
10. Enter U_{s_i} in VL(I) in the applicable line cards for region i.

The experimenter is cautioned that these relationships hold for only the cases where the absorber is not strained initially beyond its elastic limit. This restriction does not infer that SWAP-7 does not consider inelastic conditions, for it is a true elastic-plastic code based on the Grüneisen equation of state. It merely cautions the experimenter not to use the above linear relationships when initial conditions are such that the absorber is strained by the input stress wave beyond its elastic yield point in one dimensional strain.

The principal limitation of SWAP-7 results from the fact that it is restricted to longitudinal stress waves and a unidirectional cross section through the material composite. Accurate solutions are therefore limited to geometries having axial symmetry and radial dimensions large enough to preclude the perturbation of the longitudinal stress wave by lateral strains. Semiconductor devices such as transistors and integrated circuits possess the geometries that lend themselves to SWAP-7 except that, in the silicon dice, results become less accurate as the solution progresses beyond initial reflection of the stress wave from the dice surfaces. This becomes obvious when one considers the fact that strains originating from the remote edges of headers and substrates take considerably longer to propagate to the point of silicon die attachment than do strains that are nucleated at the die periphery. For

solutions that continue beyond initial reflection of the stress wave, a two-dimensional code such as TOODY[11] should be used.

Several output options are made available to the analyst by SWAP-7. A graphic presentation is provided of the distance-time (x-t) plot that shows the locations of all interactions, the real time of the interactions, and the velocities of resultant shocks. The program also automatically prints a listing of this information along with edits of stress-distance information at selected real times. Both hard-copy and movie-film outputs of stress-distance profiles at regular time intervals are also available. The latter offers the experimenter the most insight on the response of his particular device to stress waves.

---

[11] Ibid.

BIBLIOGRAPHY

1. Barker, L. M., and Lundergan, C. D., "Dynamic Response of Aluminum," JAP, V. 35, No. 4, 1203-1212, April 1964.

2. Berker, L. M., SWAP-7: A Stress-Wave Analyzing Program, Sandia Corporation Report SC-RR-67-143, April 1967.

3. Butcher, B. M.; Barker, L. M.; Munson, D. E.; and Lundergan, C. D.; "Influence of Stress History on Time-Dependent Spall in Metals," AIAA Journal, June 1964.

4. Graham, R. A.; Neilson, F. W.; and Benedick, W. B.; Piezoelectric Current from Shock-Loaded Quartz—A Sub-microsecond Stress Gauge," JAP, V. 36, No. 5, 1775-1783, May 1965.

5. Graham, R. A., and Hutchison, R. E., "Thermoelastic Stress Pulses Resulting from Pulsed Electron Beams, Applied Physics Letters, V. 11, No. 2, 15 July 1967.

6. Jones, O. E.; Neilson, F. W.; and Benedick, W. B.; "Dynamic Yield Behavior of Explosively Loaded Metals Determined by a Quartz Transducer Technique," JAP, V. 33, No. 11, 3224-3232, November 1962.

7. Kolsky, H., Stress Waves in Solids, Clarendon Press, 1953.

8. Peters, R. L., Materials Data Nomographs, Reinhold Publishing Corp., 1965.

9. Rice, M. H.; McQueen, R. G.; and Walsh, J. M.; Solid State Physics, edited by F. Seitz and D. Turnbull, Academic Press, Inc., New York, 1958, V. 6, p. 1.

10. Sokolnikoff, I. S., and Redheffer, R. M., Mathematics of Physics and Modern Engineering, McGraw-Hill Book Co. New York, 1958.